Contents lists available at ScienceDirect

Current Opinion in Solid State & Materials Science

journal homepage: www.elsevier.com/locate/cossms

Exploring photosensitive nanomaterials and optoelectronic synapses for neuromorphic artificial vision

Hyun-Haeng Lee [a,1], Jun-Seok Ro [b,1], Kwan-Nyeong Kim [a,1], Hea-Lim Park [b,*], Tae-Woo Lee [a,c,d,*]

[a] Department of Materials Science and Engineering, Seoul National University, Seoul 08826, Republic of Korea
[b] Department of Materials Science and Engineering, Seoul National University of Science and Technology, Seoul 01811, Republic of Korea
[c] Institute of Engineering Research, Interdisciplinary Program in Bioengineering, Research Institute of Advanced Materials, Soft Foundry, Seoul National University, 1 Gwanak-ro, Gwanak-gu, Seoul 08826, Republic of Korea
[d] SN Display Co., Ltd., Seoul, 08826, Republic of Korea

ABSTRACT

Artificial vision systems will be essential in intelligent machine-vision applications such as autonomous vehicles, bionic eyes, and humanoid robot eyes. However, conventional digital electronics in these systems face limitations in system complexity, processing speed, and energy consumption. These challenges have been addressed by biomimetic approaches utilizing optoelectronic synapses inspired by the biological synapses in the eye. Nanomaterials can confine photogenerated charge carriers within nano-sized regions, and thus offer significant potential for optoelectronic synapses to perform in-sensor image-processing tasks, such as classifying static multicolor images and detecting dynamic object movements. We introduce recent developments in optoelectronic synapses, focusing on use of photosensitive nanomaterials. We also explore applications of these synapses in recognizing static and dynamic optical information. Finally, we suggest future directions for research on optoelectronic synapses to implement neuromorphic artificial vision.

1. Introduction

Artificial vision systems that can process optical signals at high speed and with high precision are increasingly in demand for applications in machine vision, including autonomous vehicles, bionic eyes, and humanoid robot eyes [1,2]. However, conventional digital systems use the von Neumann architecture, in which image sensors, processors, and memories are physically separated (Fig. 1a) [3,4]. In these systems, sensors first convert optical signals to analog electrical signals, which are then converted to digital and binary electrical signals before being transferred to central processing units for classification. Thus, signal processing requires data conversion, transfer, and classification; these sequential processes slow the system and increase its energy consumption. Consequently, the utility of artificial vision systems has been constrained.

As an alternative, biological vision systems offer efficient processing capability. The photoreceptor cells and neurons in the retina enable to both sense optical signals and to perform pre-processing functions such as noise reduction, contrast increase, and motion detection [5–8]. After

being stimulated by light, neurons transmit chemical signals through a network of interconnected synapses. Repeated stimulation alters the strength of the connections between pre-synaptic and post-synaptic neurons; this adaptability, known as synaptic plasticity, enables the retina to perform pre-processing [9]. Pre-processed signals are transmitted to the brain's visual cortex for higher-level processing tasks, including recognition, learning, and memory. This integration of sensing and information pre-processing functions within the retina significantly reduces the amount of data transmitted to the brain [8]. Furthermore, the synapses react only when stimulated, so they do not operate 'sequentially' under a constant-rate clock as in the von Neumann architecture [10]. This 'event-driven' analog processing ability reduces energy cost and increases processing speed. Therefore, biomimetic approaches that replicate the structure and functionality of biological vision systems have potential to realize intelligent and efficient artificial vision systems.

Inspired by these retinal functions, optoelectronic synapses have been developed to combine sensory and pre-processing functions in a single device (Fig. 1b). These devices convert optical signals to electrical

signals in real time, and show synaptic plasticity in response to various types of information (e.g., wavelength, light intensity, light-pulse frequency) in the input signals [11,12]. Beyond silicon-based electronics, various non-silicon photosensitive materials (e.g., metal oxides, perovskites, organic materials) have been engineered to achieve retinal functions [12–16]. While these advances have achieved synaptic functions, operation in broader wavelengths with high responsivity and detectivity is still in demand.

One method to increase this range is to confine the light-matter interactions to the nanoscale. This approach is useful because photosensitive nanomaterials have a tunable bandgap, high absorption coefficient, and large surface area for light absorption [11,17–19]. Despite the advantages of nanomaterials for optoelectronic synapses, practical image-processing tasks require increased accuracy in recognizing images in the full spectral range, and in detecting the movement of objects in real time.

In this review, we explore recent progress in the development of optoelectronic synapses for artificial vision, with a focus on the use of photosensitive nanomaterials. We introduce representative nanomaterials and the operational principles of optoelectronic synapses that use these materials. Then we review applications of optoelectronic synapses that mimic the functionality of the biological vision system, including the recognition of both static and dynamic optical input. Lastly, we highlight the remaining challenges and future research directions of optoelectronic synapses for artificial vision.

## 2. Nanomaterial-based optoelectronic synapses

Optoelectronic synapses are designed in two-terminal and three-terminal device architectures to emulate the functionalities of biological vision systems by exploiting the photophysical properties of nanomaterials. Traditional photodetectors quickly lose output currents after the input ceases, whereas optoelectronic synapses can retain the current levels with only gradual decay; this trait mimics the synaptic plasticity of biological nervous systems. The synaptic plasticity of optoelectronic synapses relies on the behavior of photogenerated charge carriers that are generated by the interaction between nanomaterials and optical inputs [11].

Synaptic plasticity occurs when stimulation of the material changes the device conductance, i.e., its 'synaptic weight'. In this review, we classify synaptic plasticity into short-term plasticity (STP), and long-term plasticity (LTP) [20–22]. This classification depends on the volatility of the updated conductance, referred to as synaptic weights. STP represents transient synaptic weight changes, which typically have decay times τ_{decay} of a few milliseconds to seconds. STP enables temporal integration of input stimuli [23–26]. LTP represents a more enduring alteration in synaptic plasticity, with τ_{decay} of minutes or longer. [27,28]. LTP enables high-level cognitive functions, including pattern recognition and memory formation. Achieving synaptic plasticity that meets the requirements of specific applications requires careful choices of materials and of device configurations [11,29]. This section will present various photosensitive nanomaterials and device operation mechanisms of optoelectronic synapses.

2.1. Photosensitive nanomaterials in optoelectronic synapses

Nanomaterials have structures that are typically less than a micron, and can confine light-matter interactions to this scale (Fig. 2a) [30]. This combination of structural and optical properties enables optoelectronic synapses to have advantages such as broad-spectrum photoresponsivity, high carrier mobility, and flexibility [11,31,32]. The following subsections present various zero-dimensional (0D; e.g., quantum dots, nanoparticles), one-dimensional (1D; e.g., nanowires, nanofibers) and two-dimensional (2D; e.g., transition-metal dichalcogenides, carbon
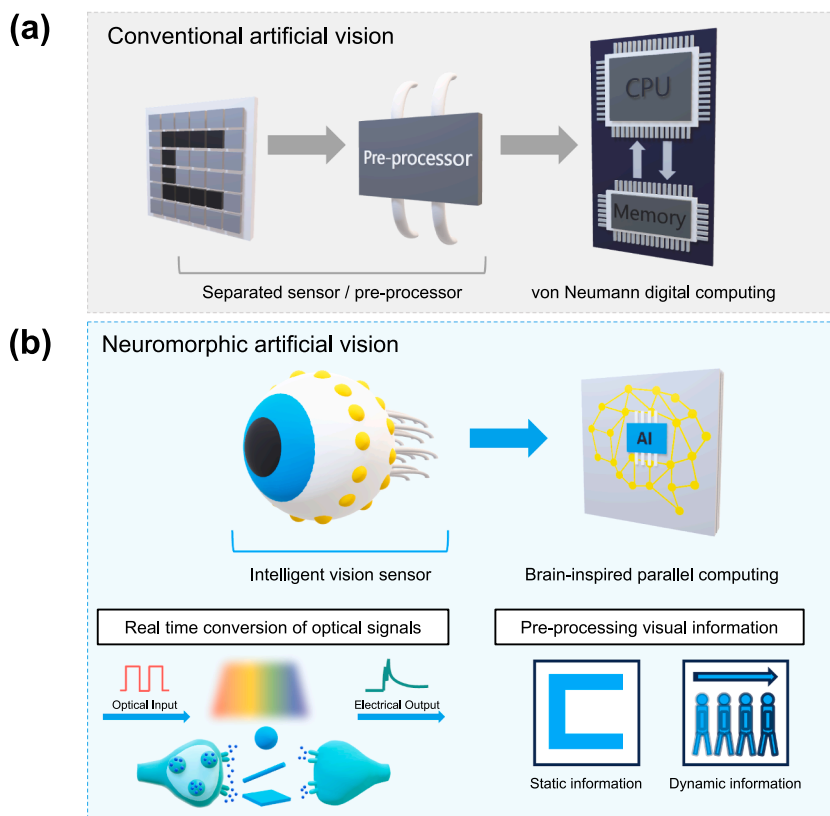
Fig. 1. Optoelectronic synapses for neuromorphic artificial vision. (a) Schematic illustration of conventional artificial vision system composed of separate image sensors, pre-processors, and von Neumann digital computing units. (b) Schematic illustration of neuromorphic artificial vision system driven by optoelectronic synapses that use nanomaterials.
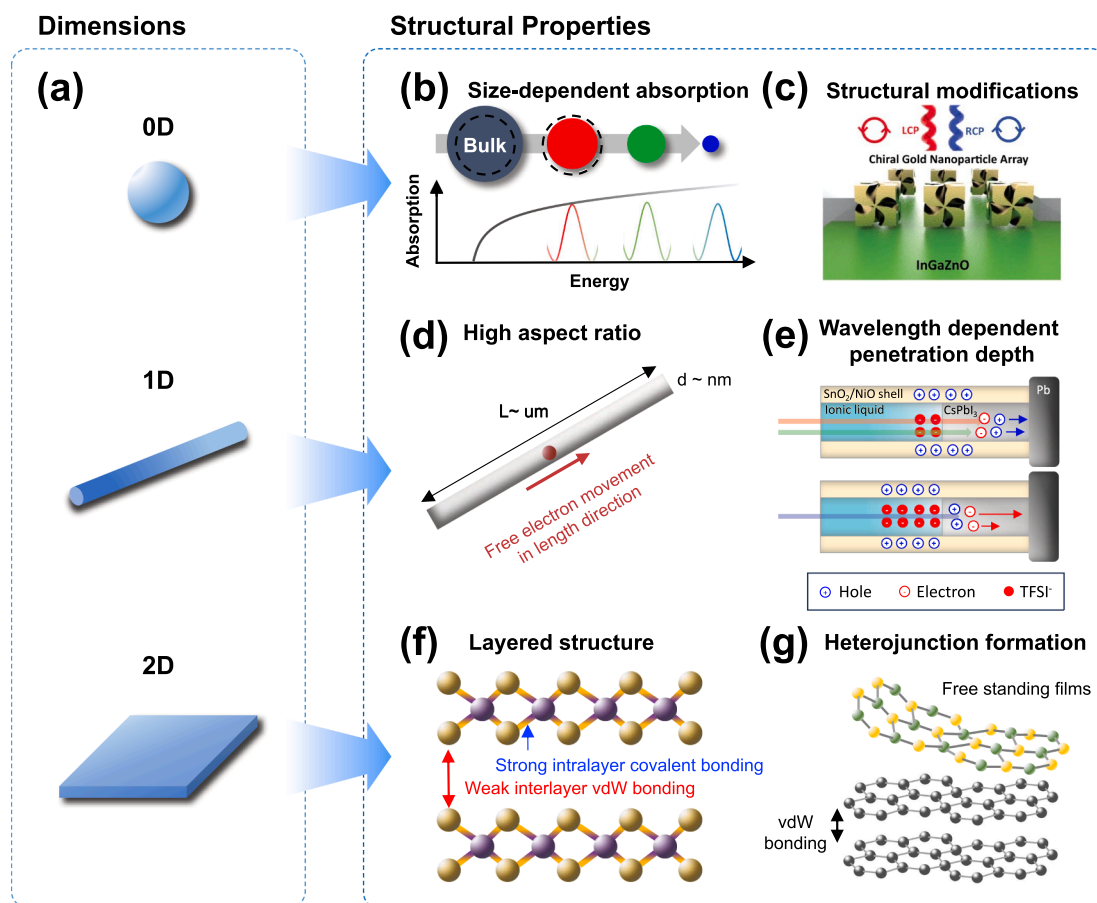
Fig. 2. Photosensitive nanomaterials and their structural properties. (a) Schematic figures of 0D, 1D and 2D nanomaterials. (b) Size-dependent absorption wavelength of QDs. As their size decreases, wavelength of absorbed light decreases. (c) Schematic figure of structure-modified chiral gold nanoparticle layered onto InGaZnO channel to distinguish left/right- circularly polarized light. Reprinted with permission from [39] CC BY-NC 4.0. (d) Schematic figure of 1D NWs. They have high aspect ratio, and photogenerated carriers move freely in the axial direction. (e) Wavelength-dependent penetration, and charge carrier motion within $CsPbI_3$ nanowires (NWs). Holes generated in the NWs can be injected into the NiO shell, where they create a positive surrounding gate effect on the NW. At long (red, green) and short (blue) wavelengths, the holes in the NiO shell can be balanced by $TFSI^-$ ions from the ionic liquid, which partially and fully neutralize the positive gate effect, respectively. This process results in a reversal of photocurrent polarity under red/green and blue light. (f) Schematic figure of 2D materials. Their layers have strong covalent bonds in-plane but weak van der Waals forces between planes. (g) Schematic figure of van der Waals heterojunction formed by 2D materials; van der Waals interaction can enable monolithic integration of 2D materials with various surfaces. (For interpretation of the references to color in this figure legend, the reader is referred to the web version of this article.)

nitride (C_3N_4)) photosensitive nanomaterials, with focus on their structural properties.

2.1.1. 0D materials

0D materials are nanoparticles (NPs) or quantum dots (QDs) that have nanometer scales in three dimensions. These materials include silicon, perovskites, and group II-VI (e.g., CdS, CdSe) compounds, and can be synthesized using bottom-up fabrication methods [18,33,34]. 0D materials offer three notable properties: high surface-to-volume ratio, controllable bandgap through precise size control, and the potential for surface functionalization to enhance optical and electronic properties.

A high surface-to-volume ratio increases light-absorption efficiency by increasing the surface area that is exposed to incident light. This trend increases the opportunities for photons to interact with the surface [11,32,35].

Controlling the size of the 0D NP to be comparable to or smaller than the Bohr exciton diameter enables tuning of the bandgap by confining excitons, and thereby provides an ability to respond to specific wavelengths (Fig. 2b). [36–38] This characteristic has been exploited to fabricate a layer composed of QDs of three different sizes: 7.1-nm CdSe that are sensitive to red light, 4.4-nm CdSe that are sensitive to green light, and 3.3-nm CdS that are sensitive to blue light [34]. Control of the

mixing ratio of the QDs in the film yielded distinct responses to different colors of light.

Structural modifications of 0D NPs can surpass the detection capabilities of the human visual system. For instance, chiral gold NPs can be fabricated in intricate and twisted chiral structures; they develop plasmonic resonances and thus respond selectively to specific wavelengths. This chiral configuration affects their interaction with light, particularly with circularly-polarized light. As a result, they generate electrons differently under right circularly-polarized light than under left circularly-polarized light (Fig. 2c) [39].

2.1.2. 1D materials

In 1D materials such as nanowires (NWs) and nanorods, charges can move freely only in the length direction (Fig. 2d) [32]. 1D materials are primarily produced using bottom-up techniques with various semiconductors, including metal oxides (e.g., ZnO, SnO_2, $InGaO_3(ZnO)_3$, In_2O_3), III-V compounds (e.g., InAs, InGaAs), and perovskites (e.g., $CsPbI_3$) [2,19,40–45]. The 1D materials offer two notable properties: a high surface-to-volume ratio and high aspect ratio.

The high surface-to-volume ratios of 1D materials yield a rich supply of surface defect states. These states impede radial-direction motion of photogenerated charge carriers, and thus impedes their rapid

recombination. This impediment extends carrier lifetimes and increases photoconductive gain [46].

The high aspect ratio of 1D materials is a consequence of their nanometer-scale diameters but lengths of up to micrometers. This elongated geometry allows for wavelength-dependent photoresponses. For instance, a $CsPbI_3$ NW array showed bidirectional synaptic behavior in response to different wavelengths of incident light. The location at which electron-hole pairs were generated within the NW varied depending on the penetration depths of the incident light; as a result, the photoresponses of the NWs changed as the wavelength of the incident light changed (Fig. 2e) [2]. Moreover, the high aspect ratio of 1D materials increases their absorption cross-sections to well beyond their physical size, so they can capture light effectively. This ability makes 1D materials particularly suitable for applications in photodetectors and solar cells, in which light absorption must be maximized [32,47].

2.1.3. 2D materials

2D materials are characterized by their confinement of light-matter interaction in only one dimension, typically measuring just a few atomic monolayers in thickness. Various 2D materials (e.g., transition metal dichalcogenides (TMDCs), black phosphorous, C_3N_4, and perovskites) have been obtained by both top-down and bottom-up methods [48–53]. Atoms in the layers are strongly covalently bonded in-plane, whereas the layers are bonded to each other only by weak van der Waals forces (Fig. 2f) [32,54]. The 2D materials offer three notable properties: an ultrathin planar structure, thickness-dependent bandgap, and free-standing nature.

The ultrathin characteristics of 2D materials yield high switching speed and high energy efficiency. This improvement occurs because the thinness shortens the pathway for electric-field-driven diffusion of charge carriers [55]. 2D semiconductors have passivated, defect-free surfaces, and therefore maintain high charge-carrier mobility; thus they are superior to bulk materials, which have numerous nanoscale surface and internal defects that reduce charge-carrier mobility [32]. Therefore, in 2D semiconductors, carriers can be effectively controlled by modulating gate voltage; this ability suppresses noise current and reduces power dissipation in devices such as photodetectors.

2D materials span a broad range of bandgaps, i.e., from graphene, which has a bandgap of approximately 0, to hexagonal boron nitride (h-BN), which has a bandgap of ~ 6 eV. Furthermore, the bandgap is affected by the material's thickness, and therefore can be modulated by altering the number of atomic layers. For instance, the bandgap of MoS_2, a TMDC, can be adjusted from an indirect bandgap of ~ 1.2 eV to a direct bandgap of ~ 1.8 eV when reduced to a monolayer [56].

The free-standing nature of 2D materials makes them advantageous for creating van der Waals heterostructures with other materials regardless of lattice mismatch (Fig. 2g) [32,54,57]. This monolithic integration of various 2D materials leads to unique optoelectronic phenomena that originate from the structural properties of stacked layers in the nanoscale. For instance, a phototransistor in which the channel was composed of NbS_2/MoS_2 heterojunction-layer films had six times higher photoresponsivity and ten times higher detectivity than a device that used only MoS_2 as the channel. These improvements occur because by inclusion of NbS_2 layers reduces contact resistance and barrier height; these changes facilitate separation of photogenerated charge carriers and suppress their recombination [5].

Highly sensitive and scalable optoelectronic synapses require careful consideration of several key factors, including the ability to sense a wide wavelength range, efficient charge transport, and the adoption of scalable fabrication methods. Understanding the strengths and challenges of these requirements across the dimensions of nanomaterials will provide strategies for achieving high sensitivity and demonstrating practical applications.

First, absorption across a broad range of wavelengths is crucial for effective utilization of diverse optical inputs, facilitating versatile functionality. Nanomaterials of 0D, 1D, and 2D dimensions exhibit excellent absorption characteristics, with their absorbance wavelengths being tunable across a wide spectral range from ultraviolet (UV) to infrared (IR) through precise control of their physical structures [36,58,59]. These materials generally exhibit absorption coefficients in the range of 10^4 to 10^6 cm^{-1}, with no single dimensionality showing a distinct advantage over others in terms of absorption efficiency [60–67]. Thus, nanomaterials across various dimensions can be employed for the development of optoelectronic synapses, with material selection strategically guided by the specific requirements of the target applications.

Second, charge transport in optoelectronic synapses is important for high detectivity with low noise levels and fast response time [19]. Compared to 0D materials, which are limited by charge transport between ligand-capped particles, 2D and 1D materials can achieve higher charge carrier mobility due to their extended and more continuous charge transport pathways [32]. Among 2D materials, TMDCs exhibit mobility in the range of 10^1 to 10^3 cm^2/V·s, while black phosphorus and graphene can achieve superior mobility values up to 10^3 cm^2/V·s and 10^5 cm^2/V·s, respectively [68,69]. 1D materials, such as single inorganic nanowires and carbon nanotubes, exhibit charge carrier mobilities on the order of 10^2 cm^2/V·s [70–72]. On the other hand, 0D materials, such as quantum dots and nanoparticles, exhibit much lower charge carrier mobilities than 1D and 2D materials, typically ranging from 10^{-3} to 10^1 cm^2/V·s [68,73,74]. The reduced mobility of 0D materials is primarily attributed to the long organic ligands on the surface of nanoparticles, which impede efficient transport of photogenerated charge carriers. To address this limitation of low mobility, 0D materials are generally integrated with charge transporting materials with higher mobilities such as carbon nanotubes and graphene [18,19]. These heterointerfaces can effectively absorb optical input signals and subsequently transport charge carriers in the active layers of optoelectronic synapses, achieving high responsivity and detectivity of optoelectronic synapses [18,19].

Lastly, for successful commercialization and practical integration of optoelectronic synapses, ensuring the compatibility of nanomaterials with scalable and cost-effective fabrication techniques is essential. Among the various nanomaterials, 0D materials offer applicability in simple and cost-effective solution processes. Quantum dots and nanocrystals, for instance, can be synthesized via solution-based methods, such as colloidal synthesis, which are compatible with industrial mass production [37,75,76]. These materials can be easily deposited onto substrates using simple and widely accessible solution process techniques, including spin-coating, inkjet printing, and dip-coating, enabling the fabrication of large-scale films for high-density device arrays in low cost. In contrast, 1D and 2D materials often require more complex and expensive fabrication techniques. For instance, scalable array fabrication of nanowires (1D) or TMDCs (2D) typically relies on chemical vapor deposition (CVD), a process that involves high-temperature (~500 °C) and high-vacuum conditions [46,55,77,78]. While CVD enables fabrication of high quality and uniform nanomaterial film, its high-cost and complexity presents challenges for large-scale and economic production.

In conclusion, fully harnessing the diverse properties of nanomaterials requires device engineering approaches tailored to their unique characteristics. Advanced device architectures, integration strategies, and fabrication techniques should be carefully designed to maximize strengths and address limitations.

2.2. Operation mechanism and synaptic plasticity

Optoelectronic synapses modulate the conductance of the active layer in response to light illumination. To achieve this requirement, various operational mechanisms exploit the intrinsic properties of photosensitive materials in active layers or specific device configurations (Fig. 3a).

Analog conductance modulation in optoelectronic synapses can be facilitated by impeding recombination of photogenerated charge carriers and delaying neutralization of ionized oxygen vacancies. For instance, in the active layers of these devices, photogenerated electrons

(a) Operation mechanism of optoelectronic synapses
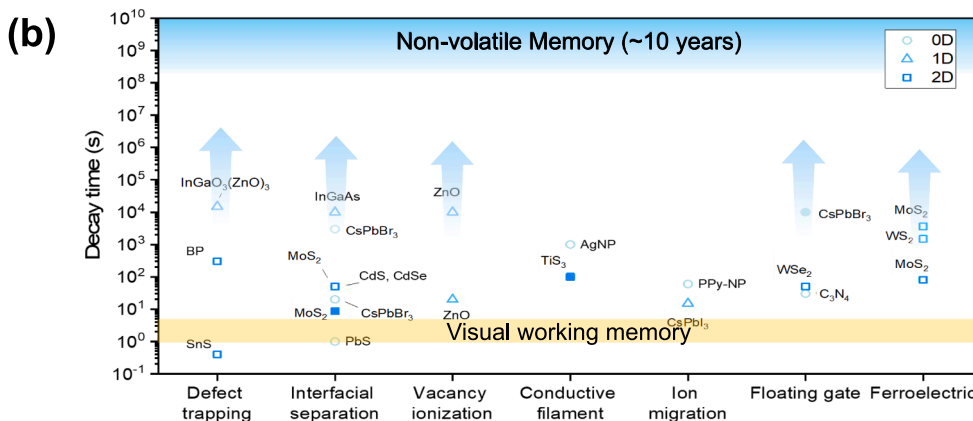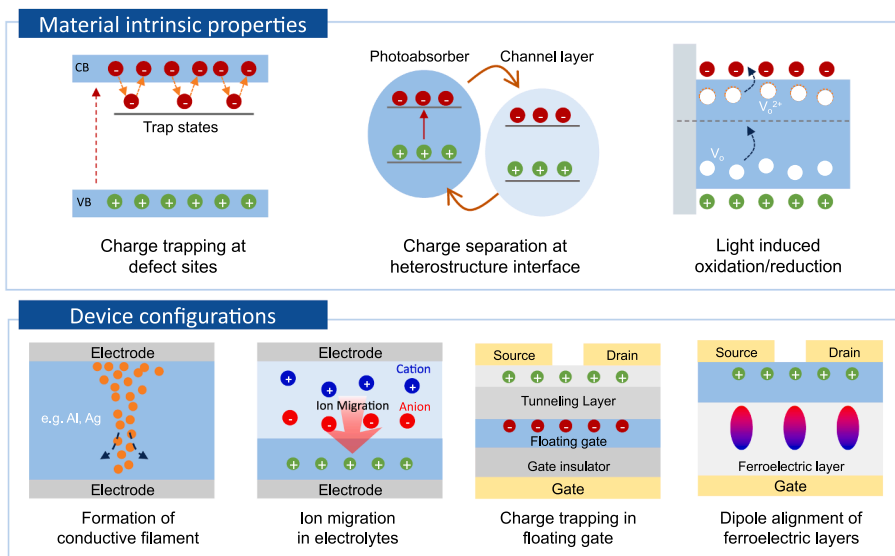
Fig. 3. Device structures and synaptic plasticity of optoelectronic synapses. (a) Illustrations of operation mechanisms in various types of optoelectronic synapses. Mechanisms that exploit the properties of photosensitive materials (top), include charge trapping at defect sites, charge separation at heterostructure interfaces between photoabsorbers and channel layers, and ionization of oxygen vacancies in the channel. Mechanisms that exploit device configurations (bottom) include formation of conductive filaments, ion migration in electrolytes, charge trapping in floating gates and dipole alignment of ferroelectric layers. (b) Benchmark of post-synaptic current retention time of optoelectronic synapses that use various materials and structures. Markers with arrows indicate that 1/e of peak level was not reached during the measurement; i.e., that they underestimate times.

and holes can be trapped within defect sites such as atomic vacancies or dangling bonds. Additionally, charge carriers can be separated and trapped in distinct layers due to a built-in electric field generated by the energy-level difference between the light absorber and the channel layer. The trapped charge carriers induce an additional electric field in the channel, and thereby increase both the charge-carrier density within the channel and the time required for charge-carrier recombination [19,33,48,51,79–81]. Moreover, in metal oxides, the energy states of oxygen vacancies exist in deep localized states above the valence band. When stimulated by light, these vacancies can release free electrons that increase the conductance of the active layer [82–84]. Neutralization of these vacancies has a large activation energy, so they can persist for relatively long times, and thereby maintain the high-conductance state.

In addition to intrinsic material properties, unique operating mechanisms are also derived from device configurations to modulate the conductance of the active layers enabling modulation of active layer conductance in response to optical inputs (Fig. 3a). A comparative analysis of different mechanisms in two- and three-terminal devices highlights their merits and challenges.

In two-terminal devices using the formation of conductive filaments,

electrical bias induces oxidation of metal electrodes, leading to the migration of metal ions to the counter electrodes that form conductive filaments within the active layers (Fig. 3a). In this operation, optical signals can either facilitate or inhibit ion conduction under electrical operation, thereby modulating the device's conductivity [85–87]. The simple structure of these devices can offer simplicity in array design and compatibility with crossbar array fabrication. However, their operation relies on electrical spike inputs, making them incapable of functioning solely through optical spike inputs [85]. Although potentiation and depression behaviors have been demonstrated through optical spike inputs where photogenerated electrons facilitate filament formation, optically induced conductance changes typically require durations in the order of tens of seconds or more [86,87]. In contrast, two-terminal memristors operating under electrical stimuli demonstrated ultrafast switching, achieving switching times as short as 120 picoseconds, enabled by the ultrathin two-dimensional hexagonal boron nitride (h-BN) switching layer [88]. However, optoelectronic synapses employing similar filament-based mechanisms have yet to achieve comparable switching speeds.

Two-terminal devices can be designed with an electrolyte layer

integrated with photosensitive nanomaterial layer to enable ion migration in response to optical stimuli (Fig. 3a). Ion migration is facilitated through two primary mechanisms: the photovoltaic effect and the photothermoelectric effect [2,89]. In the photovoltaic effect, light exposure generates charge carriers in the photosensitive layer, which, in turn, produce an electric field that induces ion migration within the electrolyte layer [2]. The photothermoelectric effect, on the other hand, involves a thermal gradient generated by light absorption in the photosensitive layer, which also induces ion migration [89]. The migrated ions generate a built-in electric field within the two-terminal device, thereby enabling photoresponsive synaptic behavior without external electrical bias. This self-driven operation is particularly advantageous for energy-efficient applications, such as bioimplantable devices where low voltage operation is important [90]. However, despite these advantages, their functionality relies on ion kinetics, which are generally slower than electrical conduction, necessitating optical input durations in the order of seconds for effective operation.

Mechanisms in three-terminal transistors, such as floating gate and ferroelectric gating, rely on charge injection dynamics and dipole switching behaviors, both of which are inherently faster than ion migration (Fig. 3a). These mechanisms enable three-terminal devices to achieve significantly faster response times compared to two-terminal devices, requiring shorter optical input durations to induce synaptic behaviors.

Photosensitive materials such as TMDCs, C_3N_4, and perovskites can be used as floating-gate layers in three-terminal optoelectronic synapses. Under illumination, photogenerated electrons or holes can tunnel through a thin layer and increase the channel conductance, while the opposite charges become trapped in a floating gate layer; the trapped charges induce an electric field that can briefly affect the channel conductance [49,52,91]. Fast modulation of conductance states was demonstrated using short optical inputs with durations of approximately 100 μs, which effectively released the trapped charges within the floating gate, enabling rapid adjustments to the device conductance [52].

Ferroelectric transistors that use ferroelectric materials (e.g., PbZr$_x$Ti$_{1-x}$O$_3$ (PZT), BaTiO$_3$, and poly(vinylidenefluoride-co-trifluoroethylene (PVDF-TrFE)) as dielectric layers with photosensitive channels exploit optical inputs to control the dipole alignment in the ferroelectric layer [92–94]. Optical input generates charges that accumulate at the interface between the channel and the ferroelectric layer; this process generates a built-in electric field which reverses dipole polarization, and thereby modulates multilevel conductance states and helps them to persist [92,93]. Short optical inputs, with durations of approximately 20 ms, effectively updated the conductance states by inducing changes in dipole polarization, thereby enabling precise modulation of multilevel conductance [92].

Despite their capability for versatile synaptic processing in response to optical spike inputs, transistor-based configurations face significant challenges related to operating voltages and bidirectional optical switching. Charge storage or release within the floating gate typically requires high operating voltages, often in the range of several tens of volts, leading to increased power consumption. Additionally, bidirectional optical switching mechanisms using ferroelectric gating have yet to be demonstrated, which is critical for enabling symmetric and reversible synaptic operations. Addressing these limitations requires further research and development to improve energy efficiency, and reliability for neuromorphic artificial vision applications.

Evaluation of synaptic plasticity involves observing the volatility of post-synaptic currents (PSCs) following illumination spikes. The volatility of synaptic response in optoelectronic devices can be analyzed by fitting exponential functions to the decay curve of PSCs. This decay behavior mimics that of biological synapses, and can serve as a metric to assess the accuracy at which artificial synaptic devices mimic the biological system [95]. The synaptic plasticity, including STP and LTP, dictates applications for which an optoelectronic synapse is suitable (Fig. 3b, Table 1).

For instance, in a two-terminal optoelectronic synapse that uses tin sulfide (SnS), optical inputs generate electrons within the SnS channel [80]. These electrons can be trapped in donor states formed by S vacancies and quickly released; these processes yield STP-dominant memory. Use of SnS can implement an optoelectronic synapse in which PSC gradually increases under successive light spikes, then decays within milliseconds after the light is turned off. This device has been used as an in-sensor reservoir for classifying Korean letters by reservoir computing.

Non-volatile memory can be achieved by using a floating-gate layer to trap charges [52]. This approach uses a heterostructure with a WSe$_2$ floating gate to trap charges and establish a non-volatile high-photoconductivity or low-photoconductivity state, depending on initial electrical settings. Subsequent light stimulation drives release of these trapped charges, and thus enables analog modulation of the non-volatile photoconductivity states. A pixel array using these devices could capture images of a moving object at intervals of Δt and perform operations using positive and negative conductivity matrices to provide information about the motion.

Despite this significant progress, achieving practical applications of intelligent pre-processing poses challenges due to the lack of guaranteed non-volatile memory, which typically require $\tau_{decay} = 10$ years for computing applications [96]. Currently, optoelectronic synapses have τ_{decay} of only hours. To achieve guaranteed non-volatility at a practical level, further advances in materials and device engineering are necessary.

3. Applications of optoelectronic synapse for artificial vision

Humans obtain ∼ 80 % of their information about the external environment by vision [97]. The retina can effectively perceive and pre-process visual data, which can be classified into static and dynamic information. Processing of static information is crucial in tasks such as medical imaging and facial recognition, in which capturing high-quality images is the primary goal [98,99]. In contrast, dynamic information processing is essential in applications such as robotic controls and autonomous vehicle navigation, in which capturing and processing moving images is important for understanding ongoing events and making timely decisions [85,100]. Optoelectronic synapses with various synaptic plasticity have been developed as pre-processors to effectively process both types of information [34]. These devices perceive the wavelength, intensity, and temporal changes of light from environments, then apply synaptic plasticity to process the perceived data; these abilities mimic the early stages of visual information processing in the human visual system [101]. These applications will be reviewed in the next subsections.

3.1. Static information recognition

As a first step toward detecting and recognizing static visual information, the classification of patterns and images has been mainly investigated. For instance, optoelectronic reservoir computing using 2D tin sulfide (SnS) optoelectronic synapses array has been used to identify Korean letters by in-sensor reservoir computing [80]. This system processes input signals directly within optoelectronic synapses, functioning as in-sensor physical reservoir devices that utilize fixed internal connections to generate complex dynamics without requiring continuous weight updates. In this system, only the output weights are trained, enabling fast and energy-efficient operation. The letters were divided into five rows, and each row was converted to a training set composed of temporal optoelectronic pulses (Fig. 4a). These signals from the individual rows were then applied to five corresponding optoelectronic synapses to determine the device conductance state (Fig. 4b). Subsequently, the integrated optoelectronic synapse array was connected to a digital readout layer implemented in software to classify temporal

Table 1
Performance Metrics of Optoelectronic Synapses Utilizing Photosensitive Nanomaterials.

Dimension	Nanomaterials	Mechanism	Wavelength	Operation intensity	Spike number(time)	Decay time* (τ_{decay})	Ref.
0D	$CsPbBr_3$	Floating Gate	365 nm	0.153 mW/cm^2	1 (30 s)	10,000 s	[91]
0D	CdS, CdSe	Interfacial Separation	405mn	5 mW/cm^2	3 (2 s)	~50 s	[34]
0D	$CsPbBr_3$	Interfacial Separation	516 nm	0.78 W/cm^2	1 (10 s)	~20 s	[19]
0D	PbS	Interfacial Separation	1100 nm	–	10 (250 ms)	~1s	[81]
0D	AgNP	Conductive filament	360 nm	21.8 mW/cm^2	1 (900 s)	~1,000 s	[87]
0D	$CsPbBr_3$	Interfacial Separation	440 nm	1.1 µW/cm^2	20 (5 s)	~3,000 s	[89]
0D	$CsPbBr_3$	Conductive filament	365 nm	0 – 2.5 mW	Not operated with optical spikes		[85]
0D	PPy-NP	Ion migration	365 nm	7.2 µW/mm^2	2 (5 s)	~ 60 s	[89]
1D	ZnO	Vacancy ionization	365 nm	0.55 mW/cm^2	1 (100 ms)	~ 20 s	[83]
1D	ZnO	Vacancy ionization	380 nm	7 mW/cm^2	1 (11 s)	~10,000 s	[82]
1D	InGaO3(ZnO)$_3$	Defect trapping	261 nm	1 mW/cm^2	1 (10 s)	~15,000 s	[43]
1D	InGaAs	Interfacial Separation	405 nm	1.1 mW/mm^2	1 (5 s)	~10,000 s	[79]
1D	$CsPbI_3$	Nanowire	405 nm	11 mW/cm^2	1 (30 s)	~15 s	[2]
2D	C_3N_4	Floating Gate	365 nm	0.38 mW/cm^2	1 (10 s)	~30 s	[49]
2D	WSe_2	Floating Gate	450 nm	4.5 nW	1 (20 ms)	~50 s	[52]
2D	TiS_3	Conductive filament	808 nm	10 mW/cm^2	–	100 s	[86]
2D	BP	Defect trapping	280 nm	2 mW/cm^2	1 (10 s)	~300 s	[48]
2D	SnS	Defect trapping	725 nm	43 mW	–	~0.4 s	[80]
2D	MoS_2	Ferroelectric	450 nm	–	1 (10 s)	~3,600 s	[92]
2D	WS_2	Ferroelectric	532 nm	10 µW	–	~1,500 s	[93]
2D	MoS_2	Ferroelectric	405 nm	19 mW/cm^2	8 (19 s)	~80	[94]
2D	MoS_2	Interfacial Separation	White	0.202 mW	–	8.61 s	[4]
2D	MoS_2	Interfacial Separation	532 nm	3.1 µW/µm^2	–	~50 s	[5]

* τ_{decay} defined as the time required for the photocurrent to decrease to 1/e of its peak value, measured from the point at which the peak is reached in response to input spikes.

sequences. After 100 training epochs, this system achieved a classification accuracy of 100 % for the Korean letters using dual optoelectronic inputs (Fig. 4c).

Noise in real-world data often distorts optical inputs, and complicates the task of accurate image recognition. Optoelectronic synapses that respond only to desired wavelengths of light offer a potential solution to reduce such noise. For this purpose, an optoelectronic synapse that uses a monolayer MoS_2 channel atop a ferroelectric $BaTiO_3$ film was developed [92]. The heterostructure had light-controlled ferroelectric polarization switching behavior, wherein accumulated charges at the MoS_2/$BaTiO_3$ interface could induce a shift in the polarization direction of the $BaTiO_3$ layer [102]. When subjected to light pulses of wavelengths 650 nm (red), 532 nm (green), and 450 nm (blue), the channel achieved distinct conductance levels: 9×10^{-3} µS for red, 5×10^{-2} µS for green, and 8 µS for blue, and demonstrated high selectivity for blue light. Additionally, the films had LTP characteristics that were wavelength-dependent; memory retention was notably high under blue illumination. This differential response can be exploited to diminish noise in multiple-colored images and to exclusively extract and store blue-light information while filtering out information from other light colors. For instance, given an image of a blue butterfly against a red and green background, the device removed the background, leaving only the blue butterfly image (Fig. 4d). These devices were further implemented as a sensor array connected to an artificial neural network to extract blue patterns from noisy images. The test images consisted of Modified National Institute of Standards and Technology (MNIST) datasets which were added with red and green Gaussian noise. Without the noise-reduction function of the sensor array, the recognition accuracy of the dataset was limited to ~ 15 %, whereas when the noise-filtering function was added, the recognition accuracy of blue patterns increased to 91 % (Fig. 4e).
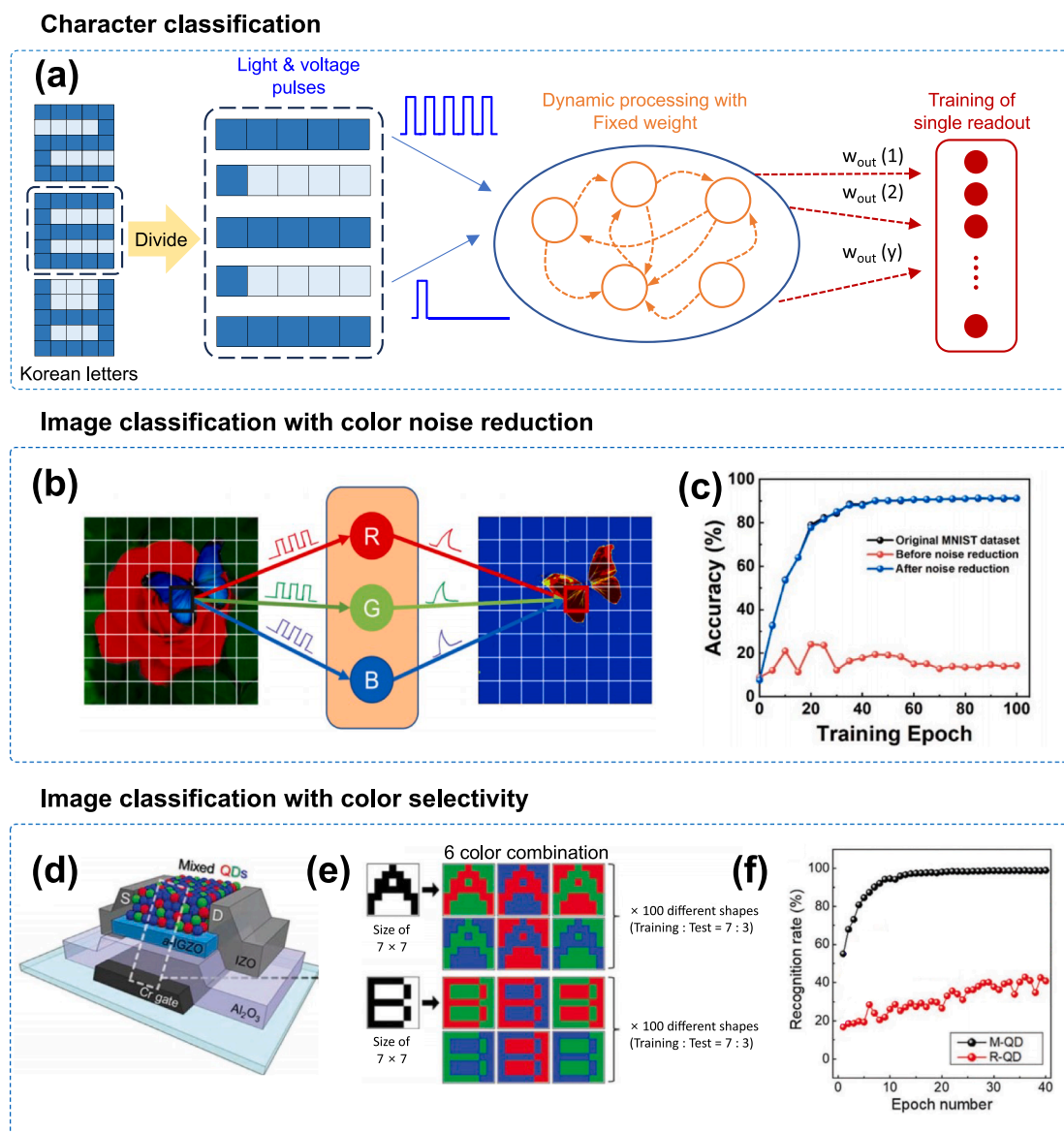
Accurate recognition of images requires an ability to discriminate among different colors across a wide spectral range [103,104]. This function can be realized in optoelectronic synapses by using a photo-absorbing layer that is composed of size-mixed QDs (M−QDs) (Fig. 4f) [34]. The M−QD layer is composed of QDs with three distinct optical band gaps that correspond to red, green, and blue, as determined by their size-dependent absorption properties. These QDs were mixed in unequal proportions inspired by the cone cells in the human eye. When stimulated by red, green, or blue light, devices that used M−QD layers

developed currents that differed by an order of magnitude. Furthermore, LTP characteristics of PSCs generated by each light source could be modulated by gate bias; this ability enabled the device to operate in wavelength-selective, non-volatile synaptic modes. This ability significantly improves over conventional optoelectronic synapses, which have fixed LTP characteristics according to each wavelength of light and cannot easily classify images with mixed-color patterns. A 7 × 7 pixelated synapse array that used M−QDs could differentiate colors in tests conducted with images of 'A' and 'B' rendered in two of the colors red, green, and blue (Fig. 4g). The system could recognize the shape of patterns by distinguishing different colors, and achieved a recognition rate > 90 %. In contrast, a similar system that used only red-sensitive QDs achieved a recognition rate of only ~ 40 % (Fig. 4h).

3.2. Dynamic information recognition

Processing of dynamic information requires the ability to detect and process temporal changes in light conditions. To achieve this ability, a smart UV-detection and blocking system was developed. C_3N_4, which strongly absorbs UV light, was used as a floating gate layer in an optoelectronic synapse to detect and process UV stimuli [49,105]. During exposure to UV light, synaptic current gradually increased over time; after the light was turned off, the current gradually declined. These synaptic properties can discern temporal information of UV exposure (e. g., duration, time, and exposure frequency) and its intensity. To develop a smart UV-detection and blocking system, an optoelectronic synapse was connected to a liquid crystal display in which the transmittance changes depending on input voltage. Due to intelligent in-sensor processing capabilities, the system underwent gradual decrease in transmittance of the display when the duration of exposure exceeded a limit; this result demonstrated smart UV detection and blocking (Fig. 5a).

Temporal information can also be exploited to recognize the movement of objects; this ability is essential for robotic vision and autonomous vehicles [26,52]. Decision-making in robot motion by considering output frequencies generated by optical stimuli has been enabled by emulating the spike responses of the biological lobula giant movement detector (LGMD) (Fig. 5b) [85]. This ability was achieved using a 20 × 20 array threshold-switching two-terminal optoelectronic synapse that had an active layer composed of a heterostructure of $CsPbBr_3$ QDs and few-layer black phosphorous nanosheets. As an object approached the

Character classification

Image classification with color noise reduction

Image classification with color selectivity

Fig. 4. Applications for static information recognition such as character classification, image classification with color-noise reduction, and image classification with color selectivity. (a) Schematic of shape classification of Korean letters by optoelectronic RC that uses 2D SnS two-terminal optoelectronic synapse arrays. The letters are separated in five rows; light and voltage pulses stimulated the five synapses serving as an in-sensor physical reservoir. The output weights are trained through software to enable letter classification. (b) Current responses of optoelectronic synapses according to input optical signals. (c) Classification accuracy for Korean letters of the optoelectronic synapse arrays using electrical and optical inputs. (a-c) Reprinted with permission from [80]. CC BY-NC 4.0. (d-e) Schematic of image classification with color noise reduction. (d) From images with blue butterfly and red and green background, the background is removed, and only blue butterfly image remains. (e) Comparisons of recognition accuracy of original MNIST dataset after and before noise reduction. (d-e) Reprinted with permission from [92]. CC BY-NC 4.0. (f-h) Schematic of image classification with color selectivity. (f) Device structure of the photosynaptic transistor that uses size-mixed quantum dots (M−QDs). (g) Examples of color combinations of pattern images of 'A' and 'B' from MNIST data set. (h) Recognition rate of color pattern images of M−QD photosynaptic system and R-QD photosynaptic system during training epochs for color pattern images. (f-h) Reprinted with permission from [34]. (For interpretation of the references to color in this figure legend, the reader is referred to the web version of this article.)

device, the number of photo-generated electrons increased; this change promoted the formation of conductive filaments and resulted in a current increase. However, the device's temperature increased due to Joule heating when the object approached too closely. When they approached nearing collision, significant Joule heating ruptured the filaments, so the current decreased (Fig. 5c). The device was integrated with an artificial LGMD neuron by using a simple circuit. These artificial neurons responded to optical inputs by converting them to trains of electrical spikes with a frequency that depended on the light intensity. The frequency-controlled system was used as the collision-avoidance function of a robotic car. Analysis of spike frequency enabled the car to detect and avoid imminent collisions (Fig. 5d).

Precise high-level classification of dynamic motion has been achieved by exploiting the long-term retention of bipolar optoelectronic synapses that use a black phosphorous/Al_2O_3/WSe_2/h-BN heterostructure (Fig. 5e) [52]. Within the synapse, non-volatile positive and negative photoconductive states could be programmed by trapping carriers in the WSe_2 floating gate by using a combination of optical and electrical pulses. By exploiting this function, positive and negative conductivity matrices could be made in the m × n pixel array of the devices. Motion was captured in a sequence of images from start time t_0 to final time t_{end}, so differencing images captured at distinct times t_i and $t_i + \Delta t$ provided insights into the motion between the two images. Specifically, images detected at t_1 and $t_1 + \Delta t$ can be multiplied by

Smart UV detection

Collision avoidance
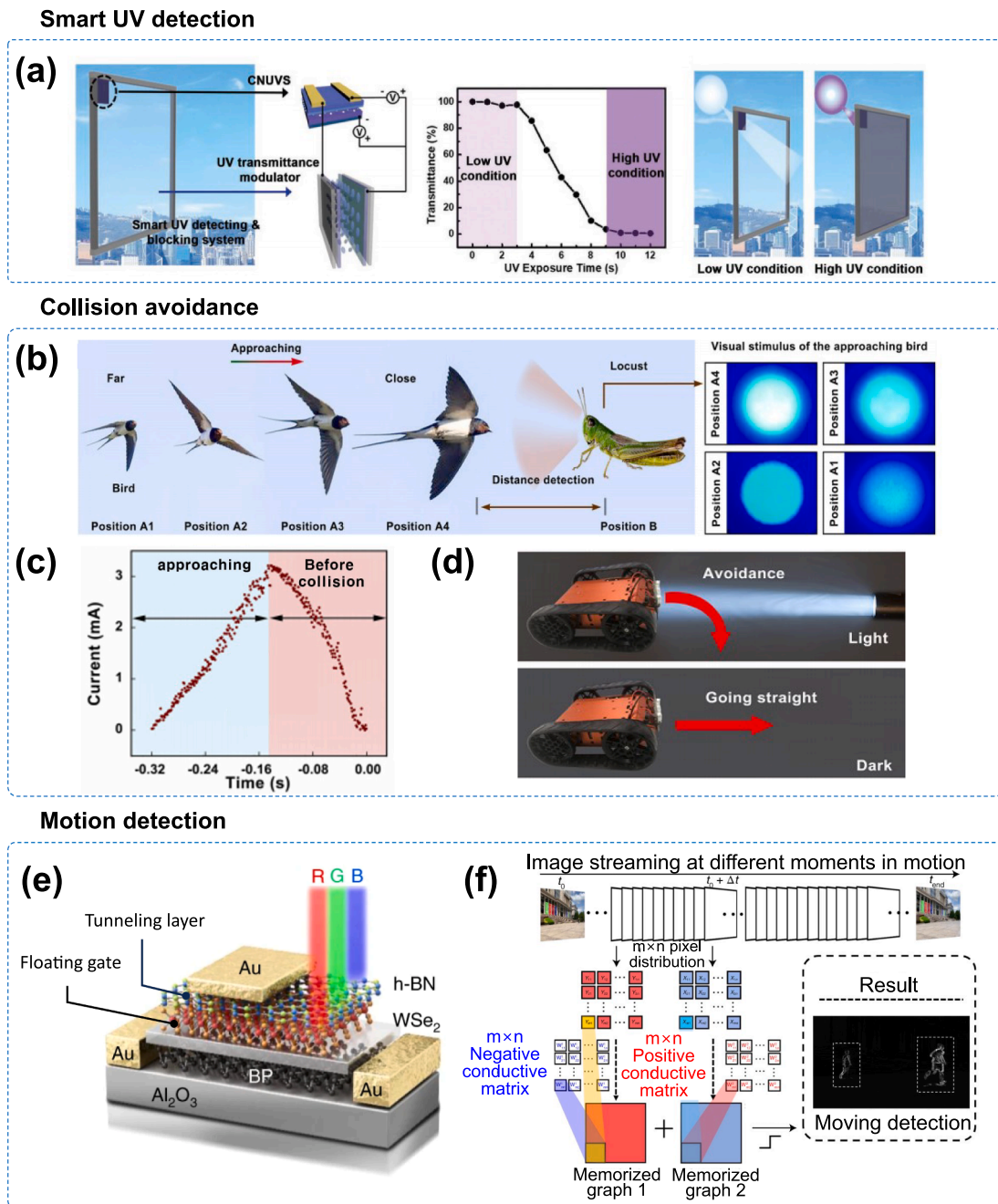
Motion detection

Fig. 5. Applications for dynamic information recognition such as Smart UV detection, collision avoidance, and motion detection. (a) Smart system to detect and block UV; UV-responsive synaptic transistors using C_3N_4 integrated with UV-transmittance modulator. Transmittance of UV rays in smart UV detection and blocking system as a function of duration of UV exposure. Reproduced with permission from [49]. (b-d) Schematic of collision-avoidance application. (b) Schematic of collision-prevention application; bird approaching LGMD neurons of locust (left) and snapshots detected as increasing light intensity as bird moves from position A1 to position A4 (right). (c) As the object approaches, the device current increases to a peak, then decreases just before the collision. (d) Schematic of collision-avoidance decision-making of LGMD neurons in a robotic car due to ability to process optical signals. (b-d) Reproduced with permission from [85]. CC BY 4.0. (e-f) Schematic of motion-detection application. (e) Device structure of an 2D retinomorphic device. The application of negative (positive) gate voltage could induce electrons of the metal gate (WSe_2 layer) to tunnel through the h-BN layer into the WSe_2 layer (metal gate), leaving the electrons (holes) trapped within the WSe_2 layer. Subsequent optical input coupled with positive (negative) gate voltage could release the trapped charge carriers to generate positive (negative) photoconductivity effects. (f) Illustration of motion detection by 2D retinomorphic device. The m × n motion image pixels at a certain frame are multiplied by the m × n positive and negative conductance matrix of the device array and summed to obtain the processed pixel output, which allows detection of object motion. (e-f) Reproduced with permission from [52].

positive and negative conductivity matrices, respectively, then summed to derive motion-related data (Fig. 5f). In the absence of object movement during Δt, pixels would be considered as noise and subtracted. However, if an object moved during Δt while the background remained nearly stable, the pixels that correspond to the moving object can be detected and recognized.

3.3. Energy efficiency of neuromorphic vision systems

Processing static and dynamic information through optoelectronic

synapses offers a promising approach to reducing energy consumption, inspired by the low energy operations of the human brain. This section highlights the event-driven analog processing capabilities of optoelectronic neuromorphic devices, which offer reduced energy consumption when compared to von Neumann architectures and biological vision systems. We provide quantitative analyses of energy consumption for both individual devices and integrated systems, offering a comparative evaluation between neuromorphic electronics and conventional digital technologies. In the quantitative comparison, we also examine optoelectronic synapses, including those not based on nanomaterials, to evaluate their practical applicability.

Biological neurons transmit signals across synapses with an energy consumption of approximately 10 femtojoules (fJ) per spike [10]. Advances in optoelectronic synapses have focused on reducing energy consumption, achieving ultra-high energy efficiencies, even surpassing those of biological systems. For instance, optoelectronic synapses utilizing MoS_2 films covered with an indium electron injection layer, have demonstrated exceptional performance, achieving ultra-low energy consumption of 68.9 attojoules (aJ) per spike which is significantly lower than the biological standard [51]. This ultra-low energy performance is primarily attributed to the surface charge doping of the MoS_2 films by the large number of electrons injected from the indium layer, which enhances the conductivity of the channel.

By leveraging the ultra-low energy consumption of optoelectronic synapses, their system-level integration can achieve significantly higher energy efficiency than conventional digital systems. For instance, a fully integrated multi-mode optoelectronic memristor (OEM) array, have demonstrated superior energy efficiency in both low-level and high-level vision applications, such as image sensory pre-processing, object tracking, and human motion recognition, outperforming conventional systems utilizing graphics processing units (GPUs) [106]. This system incorporates a 128 × 8 crossbar array of one-transistor-one-OEM (1T1OEM) cells integrated with Si complementary metal-oxide-semiconductor (CMOS) circuits. The OEMs, composed of a $Pd/TiO_x/ZnO/TiN$ material stack, enable multiple functionalities, including electronic memristor, dynamic OEM, and non-volatile OEM modes, modulated by optical and electrical stimuli. These multiple modes enable energy-efficient performance in tasks ranging from sensory pre-processing to advanced object recognition within a single array.

In image pre-processing tasks, the system utilizes the non-volatile-OEM mode, achieving a recognition accuracy of 96.1 % for noisy datasets, closely aligning with the 97 % accuracy of NVIDIA H100 GPUs on standard, noise-free datasets. Notably, the energy consumption of the OEM system was measured to be 94.2 nJ, significantly lower than the 345.8 nJ required by GPUs primarily due to higher energy efficiency per operation of the OEM system. In high-level tasks such as object tracking, the hybrid OEM system integrating dynamic sensing with dynamic-OEM and template storage using non-volatile-OEM, operates with only 23.9 nJ energy consumption, while GPUs require 85.6 nJ for comparable tasks. Accuracy levels are maintained at 96.1 % for the OEM system versus 97.4 % for GPUs. The ability of OEM system to achieve this high accuracy while maintaining low energy consumption is attributed to its non-volatility, which enable ultra-low energy consumption of approximately 0.18 picojoules per operation.

Finally, in human motion recognition, a fully OEM-based reservoir computing framework was employed, utilizing dynamic-OEM devices in the reservoir layer, and an electronic memristor readout layer for classification. Under potential optimized conditions using short input spikes (10 μs), the total energy consumption of the OEM system was measured to be 24.8 nJ, accounting for light stimulation, reservoir layer operations, transimpedance amplification conversion, and the output layer operations. In contrast, GPU-based systems rely on a CMOS sensor component comprising a photodetector, transimpedance amplifier, and buffer circuits, integrated with the GPU. This external sensing setup results in significantly higher energy consumption of 522.3 nJ, with 517 nJ attributed to the energy-intensive CMOS sensor. The OEM system's integration of sensing and processing into a single framework eliminates the need for external CMOS sensors, offering a significant advantage in energy efficiency.

The exceptional energy efficiency of OEM-based neuromorphic systems stems from their ultra-low energy consumption per operation and their seamless integration of in-sensor reservoir computing, eliminating the need for bulky, energy-intensive external sensors. Further reductions in energy consumption can potentially be achieved by incorporating nanomaterial-based optoelectronic synapses, which offer energy efficiencies extending to attojoules per spike [51]. Although nanomaterial-based optoelectronic synapses still require further development for array integration and mass production, the neuromorphic artificial vision platforms utilizing nanomaterials have great potential to overcome the limitations of bulky and high-energy GPU-based systems.

4. Conclusion and outlook

This review has explored recently-developed optoelectronic synapses that use photosensitive nanomaterials for bioinspired artificial vision systems. These devices exploit the unique photophysical properties of nanomaterials and use pre-processing functions to mimic biological vision for efficient information processing. However, to accurately recognize optical signals in diverse wavelengths with high resolution, and to detect the movements of objects, several key challenges must be addressed. Here, we highlight the key challenges and perspectives of optoelectronic synapses.

Firstly, the operation wavelength range of optoelectronic synapses should be broadened. Optoelectronic synapses developed to date are limited in their detection range to the ultraviolet to near-infrared spectrum (254 nm $\leq \lambda \leq$ to 2 μm), so their applicability is restricted to specialized applications (Fig. 6a) [108,109]. Widening of the spectral detection ability would significantly expand their applicability in fields such as non-destructive analysis (Far-IR, 3 μm $\leq \lambda \leq$ 1,000 μm) and biological imaging (X-ray, 0.01 $\leq \lambda \leq$ 10 nm) (Fig. 6) [54,110,111]. To achieve widening, novel materials must be identified, and engineering techniques must be developed to tailor the dimensions and structures of the nanomaterials to create bandgaps that can be tuned over a broad range. Precise wavelength discrimination and accurate imaging also require optimization of device structures and material interfaces.

Secondly, a significant challenge to the use of optoelectronic synapses in artificial vision is demonstrating high resolution image-processing through highly-integrated arrays (Fig. 6b). Automotive CMOS cameras—which are designed for recognizing distant traffic information—employ 8-megapixel image sensors (e.g., OmniVision's OX08B24C or Sony's IMX 324) of dimensions within a few micrometers range [112]. Additionally, emulating human vision, which involve > 10^5 photoreceptors cm^{-2} in the retina, demand great increase in device density. Recent advancements in optoelectronic synapses have achieved very-large-scale integration levels, with optoelectronic synapse arrays reaching densities of 4.1×10^5 pixels cm^{-2}, comparable to human photoreceptors [113]. However, even though high resolution patterning techniques have been developed, their application in neuromorphic vision systems still utilize only a small subset of arrays, rather than fully leveraging the entire array. Realizing high-resolution image-processing with optoelectronic synapses will therefore require not only advanced fabrication techniques but also system-level approaches to enable real-time operation of high-density arrays.

Thirdly, to apply optoelectronic synapses in wearable and implantable applications, these devices must match the softness and stretchability of biological skin and tissues (Fig. 6b). Recent progress has resulted in development of stretchable optoelectronic synapses that use intrinsically-stretchable block copolymers and perovskite QDs; the synapses have demonstrated both STP and LTP under tensile strains up to 60 % [114]. However, demonstrating bio-hybrid optoelectronic synapses that directly interface with the biological eye remains challenging due to strain-induced performance variations, mismatches in
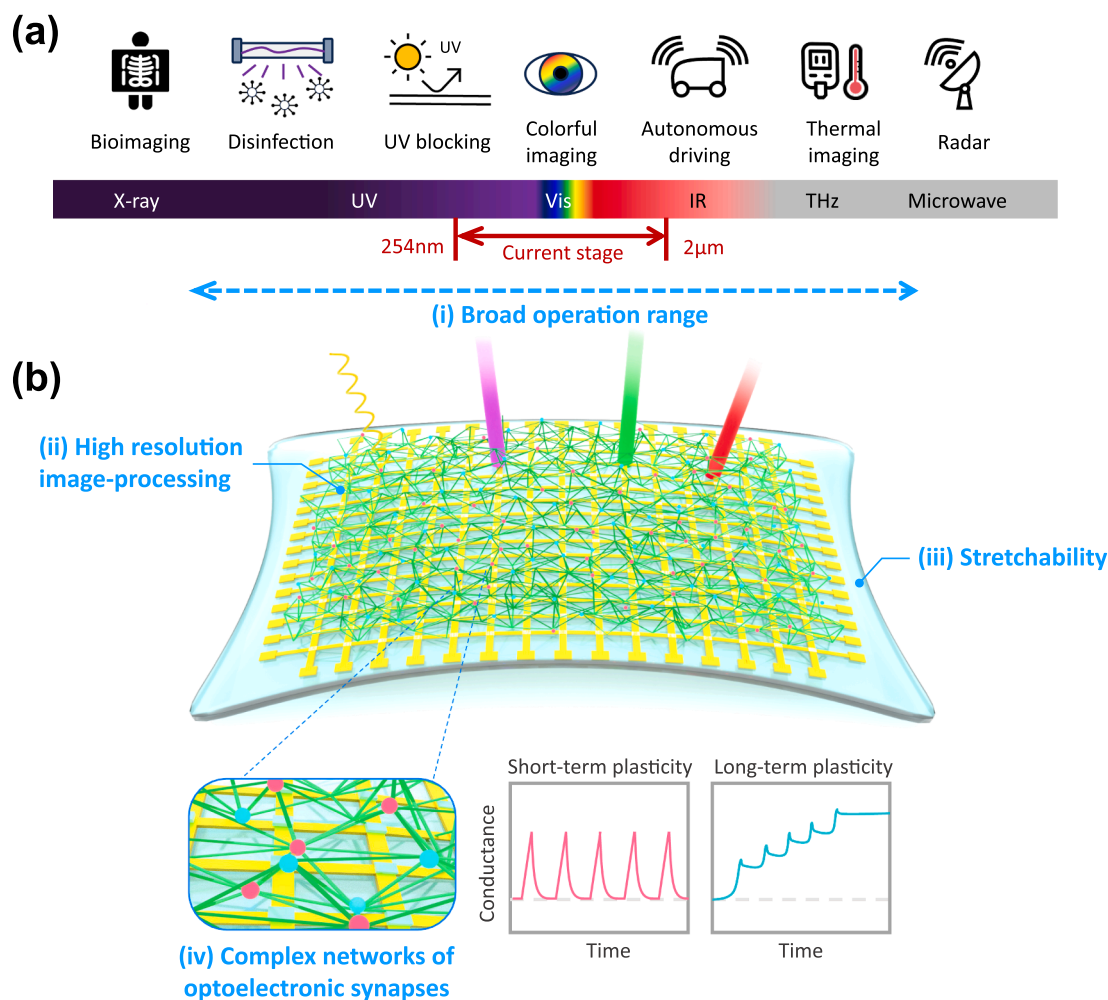
Fig. 6. Perspectives on development of optoelectronic synapses for neuromorphic artificial vision. (a) Examples of applications according to various wavelengths. (b) Challenges of optoelectronic synapses for development of practical vision systems. UV, ultraviolet; Vis, visible; IR, infrared; THz, terahertz.

softness, and structural incompatibilities. Despite the high stretchability of optoelectronic synapses up to 100 %, the stretchable devices exhibited unavoidable performance variations under stretching [107]. Such variations could potentially lead to malfunctions, posing a challenge to the long-term reliability of implantable devices. Moreover, the softness (i.e., Young's modulus) of the nanomaterials should also be optimized to ensure a conformable interface with tissues during everyday movements and minimize foreign-body responses by the immune system [115]. Typically, the elastomers used to blend with photosensitive nano-materials exhibit significantly higher Young's modulus (MPa range) than do soft biological tissues such as the brain (200 Pa), muscles (1–3 kPa), and retina (20 kPa) [116–120]. To solve this discrepancy, advances in stretchable nanomaterials coupled with innovative engineering techniques are necessary. Additionally, since the human eye has a concave structure, stretchable nanomaterials, and optoelectronic synapses should be developed to adopt a similar design.

Finally, to achieve intelligent vision sensors that use optoelectronic synapses, the intricate information processing architecture of the biological vision system must be replicated (Fig. 6b). The biological retina consists of a sophisticated neural network involving over 100 million rod cells, seven million cone cells, approximately one million ganglion cells, and other cellular components that interact through adaptable synaptic connections, which convert optical signals to action potentials and pre-process raw information before sending it to the brain [121,122]. Current optoelectronic synapses successfully emulate synaptic behaviors and primary functions of the retinal cells, but

implementing the complex network of interactions found in the biological retina remains challenging. Therefore, future research should prioritize development of complex networks of huge number of optoelectronic synapses with tunable synaptic plasticity for in-sensor pre-processing through their huge number of interconnections. These neural networks should have the sophisticated ability to preprocess visual information within the sensor and extract valuable information prior to conveying it to higher-level processing units, thus replicating the functionalities of the biological retina.

In summary, use of photosensitive nanomaterials has great promise for developing optoelectronic synapses that mimic biological vision functionalities. The exceptional sensitivity and tunable properties of these materials allow for precise modulation of conductance in response to light, and thereby enable efficient processing of static and dynamic optical information. However, several limitations must be solved before practical integration in artificial vision systems is possible. Future research efforts should prioritize the design of photosensitive nanomaterials with tailored properties to achieve widen spectral sensitivity, increase device density, and optimize mechanical stretchability. Moreover, to emulate the complex information-processing structure of the biological optic nerve requires innovative device architectures that exploit the unique characteristics of these nanomaterials. If these challenges can be addressed, optoelectronic synapses may revolutionize the field of artificial vision.

Declaration of competing interest

Acknowledgments

Data availability

No data was used for the research described in the article.

References

[1] L. Mennel, J. Symonowicz, S. Wachter, D.K. Polyushkin, A.J. Molina-Mendoza, T. Mueller, Ultrafast machine vision with 2D material neural network image sensors, Nature 579 (2020) 62–66, https://doi.org/10.1038/s41586-020-2038-x.

[2] Z. Long, X. Qiu, C.L.J. Chan, Z. Sun, Z. Yuan, S. Poddar, Y. Zhang, Y. Ding, L. Gu, Y. Zhou, W. Tang, A.K. Srivastava, C. Yu, X. Zou, G. Shen, Z. Fan, A neuromorphic bionic eye with filter-free color vision using hemispherical perovskite nanowire array retina, Nat. Commun. 14 (2023) 1972, https://doi.org/10.1038/s41467-023-37581-y.

[3] D. Lee, M. Park, Y. Baek, B. Bae, J. Heo, K. Lee, In-sensor image memorization and encoding via optical neurons for bio-stimulus domain reduction toward visual cognitive processing, Nat. Commun. 13 (2022) 5223, https://doi.org/10.1038/s41467-022-32790-3.

[4] C. Choi, J. Leem, M.S. Kim, A. Taqieddin, C. Cho, K.W. Cho, G.J. Lee, H. Seung, H. J. Bae, Y.M. Song, T. Hyeon, N.R. Aluru, S.W. Nam, D.H. Kim, Curved neuromorphic image sensor array using a MoS2-organic heterostructure inspired by the human visual recognition system, Nat. Commun. 11 (2020) 5934, https://doi.org/10.1038/s41467-020-19806-6.

[5] P.Y. Huang, B.Y. Jiang, H.J. Chen, J.Y. Xu, K. Wang, C.Y. Zhu, X.Y. Hu, D. Li, L. Zhen, F.C. Zhou, J.K. Qin, C.Y. Xu, Neuro-inspired optical sensor array for high-accuracy static image recognition and dynamic trace extraction, Nat. Commun. 14 (2023) 6736, https://doi.org/10.1038/s41467-023-42488-9.

[6] B.P. O, S.A. Baccus, M. Meister, Segregation of object and background motion in the retina, Nature 423 (2003) 401–408, doi:10.1038/nature01652.

[7] T. Euler, S. Haverkamp, T. Schubert, T. Baden, Retinal bipolar cells: elementary building blocks of vision, Nat. Rev. Neurosci. 15 (2014) 507–519, https://doi.org/10.1038/nrn3783.

[8] R.H. Masland, The neuronal organization of the retina, Neuron 76 (2012) 266–280, https://doi.org/10.1016/j.neuron.2012.10.002.

[9] Y. Li, G. Shen, Advances in optoelectronic artificial synapses, Cell Rep. Phys. Sci. 3 (2022) 101037, https://doi.org/10.1016/j.xcrp.2022.101037.

[10] Y. Lee, H.L. Park, Y. Kim, T.W. Lee, Organic electronic synapses with low energy consumption, Joule 5 (2021) 794–810, https://doi.org/10.1016/j.joule.2021.01.005.

[11] N. Ilyas, J. Wang, C. Li, D. Li, H. Fu, D. Gu, X. Jiang, F. Liu, Y. Jiang, W. Li, Nanostructured materials and architectures for advanced optoelectronic synaptic devices, Adv. Funct. Mater. 32 (2022) 2110976, https://doi.org/10.1002/adfm.202110976.

[12] M. Lee, W. Lee, S. Choi, J.W. Jo, J. Kim, S.K. Park, Y.H. Kim, Brain-inspired photonic neuromorphic devices using photodynamic amorphous oxide semiconductors and their persistent photoconductivity, Adv. Mater. 29 (2017) 1700951, https://doi.org/10.1002/adma.201700951.

[13] F. Zhou, Z. Zhou, J. Chen, T.H. Choy, J. Wang, N. Zhang, Z. Lin, S. Yu, J. Kang, H. S.P. Wong, Y. Chai, Optoelectronic resistive random access memory for neuromorphic vision sensors, Nat. Nanotechnol. 14 (2019) 776–782, https://doi.org/10.1038/s41565-019-0501-3.

[14] X. Wu, Y. Chu, R. Liu, H.E. Katz, J. Huang, Pursuing polymer dielectric interfacial effect in organic transistors for photosensing performance optimization, Adv. Sci. 4 (2017) 1700442, https://doi.org/10.1002/advs.201700442.

[15] J. Lao, W. Xu, C. Jiang, N. Zhong, B. Tian, H. Lin, C. Luo, J. Travas-Sejdic, H. Peng, C.G. Duan, Artificial synapse based on organic–inorganic hybrid perovskite with electric and optical modulation, Adv. Electron. Mater. 7 (2021) 2100291, https://doi.org/10.1002/aelm.202100291.

[16] H.-M. An, H. Jang, H. Kim, S.-D. Lee, S.-H. Lee, H.-L. Park, Engineered current path of vertical organic phototransistors for smart optoelectronic applications, J. Mater. Chem. C Mater. 11 (2023) 14580–14588, https://doi.org/10.1039/D3TC02571C.

[17] D. Jariwala, A.R. Davoyan, J. Wong, H.A. Atwater, Van der Waals materials for atomically-thin photovoltaics: promise and outlook, ACS Photonics 4 (2017) 2962–2970, https://doi.org/10.1021/acsphotonics.7b01103.

[18] B. Pradhan, S. Das, J. Li, F. Chowdhury, J. Cherusseri, D. Pandey, D. Dev, A. Krishnaprasad, E. Barrios, A. Towers, A. Gesquiere, L. Tetard, T. Roy, J. Thomas, Ultrasensitive and ultrathin phototransistors and photonic synapses using perovskite quantum dots grown from graphene lattice, Sci. Adv. 6 (2020) 5225–5237, https://doi.org/10.1126/sciadv.aay5225.

[19] Q.B. Zhu, B. Li, D.D. Yang, C. Liu, S. Feng, M.L. Chen, Y. Sun, Y.N. Tian, X. Su, X. M. Wang, S. Qiu, Q.W. Li, X.M. Li, H.B. Zeng, H.M. Cheng, D.M. Sun, A flexible ultrasensitive optoelectronic sensor array for neuromorphic vision systems, Nat. Commun. 12 (2021) 1798, https://doi.org/10.1038/s41467-021-22047-w.

[20] K.N. Kim, M.J. Sung, H.L. Park, T.W. Lee, Organic synaptic transistors for bio-hybrid neuromorphic electronics, Adv. Electron. Mater. 8 (2022) 2100935, https://doi.org/10.1002/aelm.202100935.

[21] J.-S. Ro, H.-M. An, H.-L. Park, Electrolyte-gated synaptic transistors for brain-inspired computing, Jpn. J. Appl. Phys. 62 (2023) SE0801, https://doi.org/10.35848/1347-4065/acaca4.

[22] N. Kim, G.-T. Go, H.-L. Park, Y. Ahn, J. Kim, Y. Lee, D.-G. Seo, W. Lee, Y.-H. Kim, H. Yang, T.-W. Lee, Molecular tailoring to achieve long-term plasticity in organic synaptic transistors for neuromorphic computing, Adv. Intell. Syst. 5 (2023) 2300016, https://doi.org/10.1002/aisy.202300016.

[23] H.-S. Lee, J.-S. Ro, G.-M. Ko, H.-L. Park, Flexible and stretchable synaptic devices for wearable neuromorphic electronics, Flexible Printed Electron. 8 (2023) 043001, https://doi.org/10.1088/2058-8585/ad0a37.

[24] C. Li, X. Zhang, P. Chen, K. Zhou, J. Yu, G. Wu, D. Xiang, H. Jiang, M. Wang, Q. Liu, Short-term synaptic plasticity in emerging devices for neuromorphic computing, iScience 26 (2023) 106315, doi:10.1016/j.isci.2023.106315.

[25] U. Jung, M. Kim, J. Jang, J. Bae, I.M. Kang, S. Lee, Formation of cluster-structured metallic filaments in organic memristors for wearable neuromorphic systems with bio-mimetic synaptic weight distributions, Adv. Sci. 11 (2023) 2307494, https://doi.org/10.1002/advs.202307494.

[26] R.A. John, N. Tiwari, M.I. Bin Patdillah, M.R. Kulkarni, N. Tiwari, J. Basu, S.K. Bose, Ankit, C.J. Yu, A. Nirmal, S.K. Vishwanath, C. Bartolozzi, A. Basu, N. Mathews, Self healable neuromorphic memtransistor elements for decentralized sensory signal processing in robotics, Nat. Commun. 11 (2020) 4030, doi: 10.1038/s41467-020-17870-6.

[27] H. Kim, M. Kim, A. Lee, H. Park, J. Jang, J. Bae, I.M. Kang, E. Kim, S. Lee, Organic memristor-based flexible neural networks with bio-realistic synaptic plasticity for complex combinatorial optimization, Adv. Sci. 10 (2023) 2300659, https://doi.org/10.1002/advs.202300659.

[28] S. Oh, H. Kim, S.E. Kim, M.-H. Kim, H.-L. Park, S.-H. Lee, Biodegradable and flexible polymer-based memristor possessing optimized synaptic plasticity for eco-friendly wearable neural networks with high energy efficiency, Adv. Intell. Syst. 5 (2023) 2200272, https://doi.org/10.1002/aisy.202200272.

[29] H.L. Park, M.H. Kim, H. Kim, S.H. Lee, Self-selective organic memristor by engineered conductive nanofilament diffusion for realization of practical neuromorphic system, Adv. Electron. Mater. 7 (2021) 2100299, https://doi.org/10.1002/aelm.202100299.

[30] N. Baig, I. Kammakakam, W. Falath, I. Kammakakam, Nanomaterials: a review of synthesis methods, properties, recent progress, and challenges, Mater. Adv. 2 (2021) 1821–1871, https://doi.org/10.1039/d0ma00807a.

[31] M. Lee, H. Seung, J.I. Kwon, M.K. Choi, D.H. Kim, C. Choi, Nanomaterial-based synaptic optoelectronic devices for in-sensor preprocessing of image data, ACS Omega 8 (2023) 5209–5224, https://doi.org/10.1021/acsomega.3c00440.

[32] Z. Li, T. Yan, X. Fang, Low-dimensional wide-bandgap semiconductors for UV photodetectors, Nat. Rev. Mater. 8 (2023) 587–603, https://doi.org/10.1038/s41578-023-00583-9.

[33] L. Yin, C. Han, Q. Zhang, Z. Ni, S. Zhao, K. Wang, D. Li, M. Xu, H. Wu, X. Pi, D. Yang, Synaptic silicon-nanocrystal phototransistors for neuromorphic computing, Nano Energy 63 (2019) 103859, https://doi.org/10.1016/j.nanoen.2019.103859.

[34] C. Jo, J. Kim, J.Y. Kwak, S.M. Kwon, J.B. Park, J. Kim, G.S. Park, M.G. Kim, Y. H. Kim, S.K. Park, Retina-inspired color-cognitive learning via chromatically controllable mixed quantum dot synaptic transistor arrays, Adv. Mater. 34 (2022) 2108979, https://doi.org/10.1002/adma.202108979.

[35] C. Lv, F. Zhang, C. Li, Z. Li, J. Zhao, Low-dimensional optoelectronic synaptic devices for neuromorphic vision sensors, Mater. Futures 2 (2023) 032301, https://doi.org/10.1088/2752-5724/acda4d.

[36] M. Liu, N. Yazdani, M. Yarema, M. Jansen, V. Wood, E.H. Sargent, Colloidal quantum dot electronics, Nat. Electron. 4 (2021) 548–558, https://doi.org/10.1038/s41928-021-00632-7.

[37] C.R. Kagan, E. Lifshitz, E.H. Sargent, D. V. Talapin, Building devices from colloidal quantum dots, Science 353 (2016) aac5523, doi:10.1126/science.aac5523.

[38] F.P. García de Arquer, D. V. Talapin, V.I. Klimov, Y. Arakawa, M. Bayer, E.H. Sargent, Semiconductor quantum dots: Technological progress and future challenges, Science 373 (2021) eaaz8541, doi:10.1126/science.aaz8541.

[39] S.D. Namgung, R.M. Kim, Y.C. Lim, J.W. Lee, N.H. Cho, H. Kim, J.S. Huh, H. Rhee, S. Nah, M.K. Song, J.Y. Kwon, K.T. Nam, Circularly polarized light-sensitive, hot electron transistor with chiral plasmonic nanoparticles, Nat. Commun. 13 (2022) 5081, https://doi.org/10.1038/s41467-022-32721-2.

[40] L. Sun, S. Qu, Y. Du, L. Yang, L. Yi, Z. Wang, W. Xu, Bio-inspired vision and neuromorphic image processing using printable metal oxide photonic synapses, ACS Photonics 10 (2023) 242–252, https://doi.org/10.1021/acsphotonics.2c01583.

[41] G. Hu, H. An, J. Xi, J. Lu, Q. Hua, Z. Peng, A ZnO micro/nanowire-based photonic synapse with piezo-phototronic modulation, Nano Energy 89 (2021) 106282, https://doi.org/10.1016/j.nanoen.2021.106282.

[42] Y. Chen, W. Qiu, X. Wang, W. Liu, J. Wang, G. Dai, Y. Yuan, Y. Gao, J. Sun, Solar-blind SnO2 nanowire photo-synapses for associative learning and coincidence detection, Nano Energy 62 (2019) 393–400, https://doi.org/10.1016/j.nanoen.2019.05.064.

[43] Y. Meng, F. Li, C. Lan, X. Bu, X. Kang, R. Wei, S. Yip, D. Li, F. Wang, T. Takahashi, T. Hosomi, K. Nagashima, T. Yanagida, J.C. Ho, Artificial visual systems enabled by quasi-two-dimensional electron gases in oxide superlattice nanowires, Sci. Adv. 6 (2020) 6389–6400, https://doi.org/10.1126/sciadv.abc6389.

[44] B. Li, W. Wei, X. Yan, X. Zhang, P. Liu, Y. Luo, J. Zheng, Q. Lu, Q. Lin, X. Ren, Mimicking synaptic functionality with an InAs nanowire phototransistor, Nanotechnology 29 (2018) 464004, https://doi.org/10.1088/1361-6528/aadf63.

[45] P. Xie, Y. Huang, W. Wang, Y. Meng, Z. Lai, F. Wang, S.P. Yip, X. Bu, W. Wang, D. Li, J. Sun, J.C. Ho, Ferroelectric P(VDF-TrFE) wrapped InGaAs nanowires for ultralow-power artificial synapses, Nano Energy 91 (2022) 106654, https://doi.org/10.1016/j.nanoen.2021.106654.

[46] X. Chen, B. Chen, B. Jiang, T. Gao, G. Shang, S.T. Han, C.C. Kuo, V.A.L. Roy, Y. Zhou, Nanowires for UV–vis–IR optoelectronic synaptic devices, Adv. Funct. Mater. 33 (2023) 2208807, https://doi.org/10.1002/adfm.202208807.

[47] P. Krogstrup, H.I. Jørgensen, M. Heiss, O. Demichel, J. V. Holm, M. Aagesen, J. Nygard, A. Fontcuberta I Morral, Single-nanowire solar cells beyond the Shockley-Queisser limit, Nat. Photonics 7 (2013) 306–310, doi:10.1038/nphoton.2013.32.

[48] T. Ahmed, M. Tahir, M.X. Low, Y. Ren, S.A. Tawfik, E.L.H. Mayes, S. Kuriakose, S. Nawaz, M.J.S. Spencer, H. Chen, M. Bhaskaran, S. Sriram, S. Walia, Fully light-controlled memory and neuromorphic computation in layered black phosphorus, Adv. Mater. 33 (2021) 2004207, https://doi.org/10.1002/adma.202004207.

[49] H.L. Park, H. Kim, D. Lim, H. Zhou, Y.H. Kim, Y. Lee, S. Park, T.W. Lee, Retina-inspired carbon nitride-based photonic synapses for selective detection of UV light, Adv. Mater. 32 (2020) 1906899, https://doi.org/10.1002/adma.201906899.

[50] S. Seo, J.J. Lee, R.G. Lee, T.H. Kim, S. Park, S. Jung, H.K. Lee, M. Andreev, K. B. Lee, K.S. Jung, S. Oh, H.J. Lee, K.S. Kim, G.Y. Yeom, Y.H. Kim, J.H. Park, An optogenetics-inspired flexible van der waals optoelectronic synapse and its application to a convolutional neural network, Adv. Mater. 33 (2021) 2102980, https://doi.org/10.1002/adma.202102980.

[51] Y. Hu, M. Dai, W. Feng, X. Zhang, F. Gao, S. Zhang, B. Tan, J. Zhang, Y. Shuai, Y. Q. Fu, P.A. Hu, Ultralow power optical synapses based on MoS2 layers by indium-induced surface charge doping for biomimetic eyes, Adv. Mater. 33 (2021) 2104960, https://doi.org/10.1002/adma.202104960.

[52] Z. Zhang, S. Wang, C. Liu, R. Xie, W. Hu, P. Zhou, All-in-one two-dimensional retinomorphic hardware device for motion detection and recognition, Nat. Nanotechnol. 17 (2022) 27–32, https://doi.org/10.1038/s41565-021-01003-1.

[53] D.B. Velusamy, R.H. Kim, S. Cha, J. Huh, R. Khazaeinezhad, S.H. Kassani, G. Song, S.M. Cho, S.H. Cho, I. Hwang, J. Lee, K. Oh, H. Choi, C. Park, Flexible transition metal dichalcogenide nanosheets for band-selective photodetection, Nat. Commun. 6 (2015) 8063, https://doi.org/10.1038/ncomms9063.

[54] Y. Meng, J. Feng, S. Han, Z. Xu, W. Mao, T. Zhang, J.S. Kim, I. Roh, Y. Zhao, D. H. Kim, Y. Yang, J.W. Lee, L. Yang, C.W. Qiu, S.H. Bae, Photonic van der Waals integration from 2D materials to 3D nanomembranes, Nat. Rev. Mater. 8 (2023) 498–517, https://doi.org/10.1038/s41578-023-00558-w.

[55] T.-J. Ko, H. Li, S.A. Mofid, C. Yoo, E. Okogbue, S.S. Han, M.S. Shawkat, A. Krishnaprasad, M.M. Islam, D. Dev, Y. Shin, K.H. Oh, G.-H. Lee, T. Roy, Y. Jung, Two-Dimensional Near-Atom-Thickness Materials for Emerging Neuromorphic Devices and Applications, iScience 23 (2020) 101676, doi:10.1016/j.isci.2020.101676.

[56] B. Radisavljevic, A. Radenovic, J. Brivio, V. Giacometti, A. Kis, Single-layer MoS2 transistors, Nat. Nanotechnol. 6 (2011) 147–150, https://doi.org/10.1038/nnano.2010.279.

[57] A.K. Geim, I.V. Grigorieva, Van der Waals heterostructures, Nature 499 (2013) 419–425, https://doi.org/10.1038/nature12385.

[58] D. Rajska, K.E. Hnida-Gut, M. Gajewska, D. Chlebda, A. Brzózka, G.D. Sulka, Adjusting the crystal size of InSb nanowires for optical band gap energy modification, Mater. Chem. Phys. 254 (2020) 123498, https://doi.org/10.1016/j.matchemphys.2020.123498.

[59] P. Ajayan, P. Kim, K. Banerjee, Two-dimensional van der Waals materials, Phys. Today. 69 (2016) 38–44, https://doi.org/10.1063/PT.3.3297.

[60] A. Rubino, G. Lozano, M.E. Calvo, H. Míguez, Determination of the optical constants of ligand-free organic lead halide perovskite quantum dots, Nanoscale 15 (2022) 2553–2560, https://doi.org/10.1039/d2nr05109e.

[61] M. Alexandre, H. Águas, E. Fortunato, R. Martins, M.J. Mendes, Light management with quantum nanostructured dots-in-host semiconductors, Light Sci. Appl. 10 (2021) 231, https://doi.org/10.1038/s41377-021-00671-x.

[62] R. Singh, S.R. Suranagi, S.J. Yang, K. Cho, Enhancing the power conversion efficiency of perovskite solar cells via the controlled growth of perovskite nanowires, Nano Energy 51 (2018) 192–198, https://doi.org/10.1016/j.nanoen.2018.06.054.

[63] H. Wook Shin, S.J. Lee, D.G. Kim, M.H. Bae, J. Heo, K.J. Choi, W.J. Choi, J.W. Choe, J.C. Shin, Short-wavelength infrared photodetector on Si employing strain-induced growth of very tall InAs nanowire arrays, Sci. Rep. 5 (2015) 10764, doi: 10.1038/srep10764.

[64] F. Telesca, F. Signorelli, A. Tosi, Temperature-dependent photon detection efficiency model for InGaAs/InP SPADs, Opt. Express 30 (2022) 4504, https://doi.org/10.1364/oe.444536.

[65] J. Li, S. Majety, R. Dahal, W.P. Zhao, J.Y. Lin, H.X. Jiang, Dielectric strength, optical absorption, and deep ultraviolet detectors of hexagonal boron nitride epilayers, Appl. Phys. Lett. 101 (2012) 171112, https://doi.org/10.1063/1.4764533.

[66] A. Maniyar, S. Choudhary, Visible region absorption in TMDs/phosphorene heterostructures for use in solar energy conversion applications, RSC Adv. 10 (2020) 31730–31739, https://doi.org/10.1039/d0ra05810f.

[67] R. Hashemi, S. Shojaei, B. Rezaei, Z. Liu, Valley-optical absorption in planar transition metal dichalcogenide superlattices, Sci. Rep. 13 (2023) 5439, https://doi.org/10.1038/s41598-023-31950-9.

[68] Z. Zeng, Y. Wang, A. Pan, X. Wang, Ultrafast photocurrent detection in low-dimensional materials, Phys. Status Solidi - Rapid Res. Lett. 18 (2024) 2300120, https://doi.org/10.1002/pssr.202300120.

[69] F. Xia, H. Wang, Y. Jia, Rediscovering black phosphorus as an anisotropic layered material for optoelectronics and electronics, Nat. Commun. 5 (2014) 4458, https://doi.org/10.1038/ncomms5458.

[70] L. Shao, H. Wang, Y. Yang, Y. He, Y. Tang, H. Fang, J. Zhao, H. Xiao, K. Liang, M. Wei, W. Xu, M. Luo, Q. Wan, W. Hu, T. Gao, Z. Cui, Optoelectronic properties of printed photogating carbon nanotube thin film transistors and their application for light-stimulated neuromorphic devices, ACS Appl. Mater. Interfaces 11 (2019) 12161–12169, https://doi.org/10.1021/acsami.9b02086.

[71] R. Xiao, Y. Hou, Y. Fu, X. Peng, Q. Wang, E. Gonzalez, S. Jin, D. Yu, Photocurrent mapping in single-crystal methylammonium lead iodide perovskite nanostructures, Nano Lett. 16 (2016) 7710–7717, https://doi.org/10.1021/acs.nanolett.6b03782.

[72] F. Li, Y. Meng, X. Kang, S.P. Yip, X. Bu, H. Zhang, J.C. Ho, High-mobility in and Ga co-doped ZnO nanowires for high-performance transistors and ultraviolet photodetectors, Nanoscale 12 (2020) 16153–16161, https://doi.org/10.1039/d0nr03740k.

[73] E.M. Sanehira, A.R. Marshall, J.A. Christians, S.P. Harvey, P.N. Ciesielski, L.M. Wheeler, P. Schulz, L.Y. Lin, M.C. Beard, J.M. Luther, Enhanced mobility CsPbI 3 quantum dot arrays for record-efficiency, high-voltage photovoltaic cells, Sci. Adv. 3 (2017) eaao4204, doi:10.1126/sciadv.aao4204.

[74] D. Zhitomirsky, O. Voznyy, L. Levina, S. Hoogland, K.W. Kemp, A.H. Ip, S. M. Thon, E.H. Sargent, Engineering colloidal quantum dot solids within and beyond the mobility-invariant regime, Nat. Commun. 5 (2014) 3803, https://doi.org/10.1038/ncomms4803.

[75] Quantum dots make it big at last, Nat. Mater. 23 (2024) 159, doi:10.1038/s41563-024-01807-1.

[76] D.V. Talapin, J.S. Lee, M.V. Kovalenko, E.V. Shevchenko, Prospects of colloidal nanocrystals for electronic and optoelectronic applications, Chem. Rev. 110 (2010) 389–458, https://doi.org/10.1021/cr900137k.

[77] C. Jia, Z. Lin, Y. Huang, X. Duan, Nanowire electronics: from nanoscale to macroscale, Chem. Rev. 119 (2019) 9074–9135, https://doi.org/10.1021/acs.chemrev.9b00164.

[78] S.H. Choi, S.J. Yun, Y.S. Won, C.S. Oh, S.M. Kim, K.K. Kim, Y.H. Lee, Large-scale synthesis of graphene and other 2D materials towards industrialization, Nat. Commun. 13 (2022) 1484, https://doi.org/10.1038/s41467-022-29182-y.

[79] P. Xie, X. Chen, Z. Zeng, W. Wang, Y. Meng, Z. Lai, Q. Quan, D. Li, W. Wang, X. Bu, S.W. Tsang, S.P. Yip, J. Sun, J.C. Ho, Artificial visual systems with tunable photoconductivity based on organic molecule-nanowire heterojunctions, Adv. Funct. Mater. 33 (2023) 2209091, https://doi.org/10.1002/adfm.202209091.

[80] L. Sun, Z. Wang, J. Jiang, Y. Kim, B. Joo, S. Zheng, S. Lee, W.J. Yu, B.-S. Kong, H. Yang, In-sensor reservoir computing for language learning via two-dimensional memristors, Sci. Adv. 7 (2021) 1455–1469, https://doi.org/10.1126/sciadv.abg1455.

[81] X. Huang, Y. Liu, G. Liu, K. Liu, X. Wei, M. Zhu, M. Wen, Z. Zhao, Y. Guo, Y. Liu, Short-wave infrared synaptic phototransistor with ambient light adaptability for flexible artificial night visual system, Adv. Funct. Mater. 33 (2023) 2208836, https://doi.org/10.1002/adfm.202208836.

[82] Y. Ni, Y. Gong, L. Sun, L. Liu, H. Wei, Z. Xu, W. Xu, W. Xu, A low-dimensional hybrid p-i-n heterojunction neuromorphic transistor with ultra-high UV sensitivity and immediate switchable plasticity, Appl. Mater. Today 25 (2021) 101223, https://doi.org/10.1016/j.apmt.2021.101223.

[83] F. Sun, Q. Lu, L. Liu, L. Li, Y. Wang, M. Hao, C. Cao, Z. Wang, S. Wang, T. Li, T. Zhang, Bioinspired flexible, dual-modulation synaptic transistors toward artificial visual memory systems, Adv. Mater. Technol. 5 (2020) 1900888, https://doi.org/10.1002/admt.201900888.

[84] M.K. Kim, J.S. Lee, Synergistic improvement of long-term plasticity in photonic synapses using ferroelectric polarization in hafnia-based oxide-semiconductor transistors, Adv. Mater. 32 (2020) 1907826, https://doi.org/10.1002/adma.201907826.

[85] Y. Wang, Y. Gong, S. Huang, X. Xing, Z. Lv, J. Wang, J.Q. Yang, G. Zhang, Y. Zhou, S.T. Han, Memristor-based biomimetic compound eye for real-time collision detection, Nat. Commun. 12 (2021) 5979, https://doi.org/10.1038/s41467-021-26314-8.

[86] L. Liu, Z. Cheng, B. Jiang, Y. Liu, Y. Zhang, F. Yang, J. Wang, X.F. Yu, P.K. Chu, C. Ye, Optoelectronic artificial synapses based on two-dimensional transitional-metal trichalcogenide, ACS Appl. Mater. Interfaces 13 (2021) 30797–30805, https://doi.org/10.1021/acsami.1c03202.

[87] X. Shan, C. Zhao, X. Wang, S. Fu, Y. Lin, T. Zeng, X. Zhao, H. Xu, X. Zhang, Y. Liu, Plasmonic optoelectronic memristor enabling fully light-modulated synaptic plasticity for neuromorphic vision, Adv. Sci. 9 (2022) 2104632, https://doi.org/10.1002/advs.202104632.

[88] S.S. Teja Nibhanupudi, A. Roy, D. Veksler, M. Coupin, K.C. Matthews, M. Disiena, Ansh, J. V. Singh, I.R. Gearba-Dolocan, J. Warner, J.P. Kulkarni, G. Bersuker, S.K.

Banerjee, Ultra-fast switching memristors based on two-dimensional materials, Nat. Commun. 15 (2024) 2334, doi:10.1038/s41467-024-46372-y.

[89] X. Luo, C. Chen, Z. He, M. Wang, K. Pan, X. Dong, Z. Li, B. Liu, Z. Zhang, Y. Wu, C. Ban, R. Chen, D. Zhang, K. Wang, Q. Wang, J. Li, G. Lu, J. Liu, Z. Liu, W. Huang, A bionic self-driven retinomorphic eye with ionogel photosynaptic retina, Nat. Commun. 15 (2024) 3086, https://doi.org/10.1038/s41467-024-47374-6.

[90] S.W. Lee, S. Kim, K.N. Kim, M.J. Sung, T.W. Lee, Increasing the stability of electrolyte-gated organic synaptic transistors for neuromorphic implants, Biosens. Bioelectron. 261 (2024) 116444, https://doi.org/10.1016/j.bios.2024.116444.

[91] Y. Wang, Z. Lv, J. Chen, Z. Wang, Y. Zhou, L. Zhou, X. Chen, S.T. Han, Photonic synapses based on inorganic perovskite quantum dots for neuromorphic computing, Adv. Mater. 30 (2018) 1802883, https://doi.org/10.1002/adma.201802883.

[92] J. Du, D. Xie, Q. Zhang, H. Zhong, F. Meng, X. Fu, Q. Sun, H. Ni, T. Li, E. jia Guo, H. Guo, M. He, C. Wang, L. Gu, X. Xu, G. Zhang, G. Yang, K. Jin, C. Ge, A robust neuromorphic vision sensor with optical control of ferroelectric switching, Nano Energy 89 (2021) 106439, doi:10.1016/j.nanoen.2021.106439.

[93] Z.D. Luo, X. Xia, M.M. Yang, N.R. Wilson, A. Gruverman, M. Alexe, Artificial optoelectronic synapses based on ferroelectric field-effect enabled 2D transition metal dichalcogenide memristive transistors, ACS Nano 14 (2020) 746–754, https://doi.org/10.1021/acsnano.9b07687.

[94] Y. Jiang, L. Zhang, R. Wang, H. Li, L. Li, S. Zhang, X. Li, J. Su, X. Song, C. Xia, Asymmetric ferroelectric-gated two-dimensional transistor integrating self-rectifying photoelectric memory and artificial synapse, ACS Nano 16 (2022) 11218–11226, https://doi.org/10.1021/acsnano.2c04271.

[95] D.G. Seo, Y. Lee, G.T. Go, M. Pei, S. Jung, Y.H. Jeong, W. Lee, H.L. Park, S. W. Kim, H. Yang, C. Yang, T.W. Lee, Versatile neuromorphic electronics by modulating synaptic decay of single organic synaptic transistor: from artificial neural networks to neuro-prosthetics, Nano Energy 65 (2019) 104035, https://doi.org/10.1016/j.nanoen.2019.104035.

[96] K. Byun, I. Choi, S. Kwon, Y. Kim, D. Kang, Y.W. Cho, S.K. Yoon, S. Kim, Recent advances in synaptic nonvolatile memory devices and compensating architectural and algorithmic methods toward fully integrated neuromorphic chips, Adv. Mater. Technol. 8 (2023) 2200884, https://doi.org/10.1002/admt.202200884.

[97] Y.H. Jung, B. Park, J.U. Kim, T. il Kim, Bioinspired Electronics for Artificial Sensory Systems, Adv. Mater. 31 (2019) 1803637, doi:10.1002/adma.201803637.

[98] G. Llosá, Recent developments in photodetection for medical applications, Nucl. Instrum. Methods Phys. Res. A 787 (2015) 353–357, https://doi.org/10.1016/j.nima.2015.01.071.

[99] J.M. Llauradó, F.A. Pujol, D. Tomás, A. Visvizi, M. Pujol, Study of image sensors for enhanced face recognition at a distance in the Smart City context, Sci. Rep. 13 (2023) 14713, https://doi.org/10.1038/s41598-023-40110-y.

[100] J. Chen, Z. Zhou, B.J. Kim, Y. Zhou, Z. Wang, T. Wan, J. Yan, J. Kang, J.H. Ahn, Y. Chai, Optoelectronic graded neurons for bioinspired in-sensor motion perception, Nat. Nanotechnol. 18 (2023) 882–888, https://doi.org/10.1038/s41565-023-01379-2.

[101] N. Li, S. Zhang, Y. Peng, X. Li, Y. Zhang, C. He, G. Zhang, 2D semiconductor-based optoelectronics for artificial vision, Adv. Funct. Mater. 33 (2023) 2305589, https://doi.org/10.1002/adfm.202305589.

[102] T. Li, A. Lipatov, H. Lu, H. Lee, J.W. Lee, E. Torun, L. Wirtz, C.B. Eom, J. Íñiguez, A. Sinitskii, A. Gruverman, Optical control of polarization in ferroelectric heterostructures, Nat. Commun. 9 (2018) 3344, https://doi.org/10.1038/s41467-018-05640-4.

[103] S. Seo, S.-H. Jo, S. Kim, J. Shim, S. Oh, J.-H. Kim, K. Heo, J.-W. Choi, C. Choi, S. Oh, D. Kuzum, H.-S.-P. Wong, J.-H. Park, Artificial optic-neural synapse for colored and color-mixed pattern recognition, Nat. Commun. 9 (2018) 5106, https://doi.org/10.1038/s41467-018-07572-5.

[104] H.-L. Park, J. Jun, M.-H. Kim, S.-H. Lee, Introduction of helical photonic crystal insulator in organic phototransistor for enhancing selective color absorption, Org. Electron. 100 (2022) 106385, https://doi.org/10.1016/j.orgel.2021.106385.

[105] H. Ou, L. Lin, Y. Zheng, P. Yang, Y. Fang, X. Wang, Tri- *s* -triazine-based crystalline carbon nitride nanosheets for an improved hydrogen evolution, Adv. Mater. 29 (2017) 1700008, https://doi.org/10.1002/adma.201700008.

[106] H. Huang, X. Liang, Y. Wang, J. Tang, Y. Li, Y. Du, W. Sun, J. Zhang, P. Yao, X. Mou, F. Xu, J. Zhang, Y. Lu, Z. Liu, J. Wang, Z. Jiang, R. Hu, Z. Wang, Q. Zhang, B. Gao, X. Bai, L. Fang, Q. Dai, H. Yin, H. Qian, H. Wu, Fully integrated multi-mode optoelectronic memristor array for diversified in-sensor computing, Nat. Nanotechnol. (2024) 93–103, https://doi.org/10.1038/s41565-024-01794-z.

[107] C. Wang, Y. Bian, K. Liu, M. Qin, F. Zhang, M. Zhu, W. Shi, M. Shao, S. Shang, J. Hong, Z. Zhu, Z. Zhao, Y. Liu, Y. Guo, Strain-insensitive viscoelastic perovskite film for intrinsically stretchable neuromorphic vision-adaptive transistors, Nat. Commun. 15 (2024) 3123, https://doi.org/10.1038/s41467-024-47532-w.

[108] M.M. Islam, A. Krishnaprasad, D. Dev, R. Martinez-Martinez, V. Okonkwo, B. Wu, S.S. Han, T.S. Bae, H.S. Chung, J. Touma, J. Jung, T. Roy, Multiwavelength optoelectronic synapse with 2D materials for mixed-color pattern recognition, ACS Nano 16 (2022) 10188–10198, https://doi.org/10.1021/acsnano.2c01035.

[109] J. Chen, X. Liu, Q. Zhu, X. Fang, W. Xu, 2D Ca2Nb3O10 Optoelectronic Neuromorphic Device for Ultrasensitive UV-C Vision and Encrypted Communication, Adv. Funct. Mater. (2024) 2402684, doi:10.1002/adfm.202402684.

[110] K. Li, L. Xia, N.F. Liu, F. Nicoli, J. Constantinides, C. D'Ambrosia, D. Lazzeri, M. Tremp, J.F. Zhang, Y.X. Zhang, Far infrared ray (FIR) therapy: an effective and oncological safe treatment modality for breast cancer related lymphedema, J. Photochem. Photobiol. B 172 (2017) 95–101, https://doi.org/10.1016/j.jphotobiol.2017.05.011.

[111] J. Liu, P. Liu, T. Shi, M. Ke, K. Xiong, Y. Liu, L. Chen, L. Zhang, X. Liang, H. Li, S. Lu, X. Lan, G. Niu, J. Zhang, P. Fei, L. Gao, J. Tang, Flexible and broadband colloidal quantum dots photodiode array for pixel-level X-ray to near-infrared image fusion, Nat. Commun. 14 (2023) 5352, https://doi.org/10.1038/s41467-023-40620-3.

[112] Y. Li, J. Moreau, J. Ibanez-Guzman, Emergent visual sensors for autonomous vehicles, IEEE Trans. Intell. Transp. Syst. 24 (2023) 4716–4737, https://doi.org/10.1109/TITS.2023.3248483.

[113] S. Zhang, R. Chen, D. Kong, Y. Chen, W. Liu, D. Jiang, W. Zhao, C. Chang, Y. Yang, Y. Liu, D. Wei, Photovoltaic nanocells for high-performance large-scale-integrated organic phototransistors, Nat. Nanotechnol. 19 (2024) 1323–1332, https://doi.org/10.1038/s41565-024-01707-0.

[114] W.C. Chen, Y.C. Lin, C.C. Hung, L.C. Hsu, Y.S. Wu, C.L. Liu, C.C. Kuo, W.C. Chen, Stretchable photosynaptic transistor with an ultralow energy consumption conferred using conjugated block copolymers/perovskite quantum dots nanocomposites, Mater. Today 70 (2023) 57–70, https://doi.org/10.1016/j.mattod.2023.10.010.

[115] Y. Li, N. Li, W. Liu, A. Prominski, S. Kang, Y. Dai, Y. Liu, H. Hu, S. Wai, S. Dai, Z. Cheng, Q. Su, P. Cheng, C. Wei, L. Jin, J.A. Hubbell, B. Tian, S. Wang, Achieving tissue-level softness on stretchable electronics through a generalizable soft interlayer design, Nat. Commun. 14 (2023) 4488, https://doi.org/10.1038/s41467-023-40191-3.

[116] N. Adly, S. Weidlich, S. Seyock, F. Brings, A. Yakushenko, A. Offenhäusser, B. Wolfrum, Printed microelectrode arrays on soft materials: from PDMS to hydrogels, Npj Flexible Electron. 2 (2018) 15, https://doi.org/10.1038/s41528-018-0027-z.

[117] A. Roy, J. Mead, S. Wang, H. Huang, Effects of surface defects on the mechanical properties of ZnO nanowires, Sci. Rep. 7 (2017) 9547, https://doi.org/10.1038/s41598-017-09843-5.

[118] L. Hu, Q. Zhao, S. Huang, J. Zheng, X. Guan, R. Patterson, J. Kim, L. Shi, C.H. Lin, Q. Lei, D. Chu, W. Tao, S. Cheong, R.D. Tilley, A.W.Y. Ho-Baillie, J.M. Luther, J. Yuan, T. Wu, Flexible and efficient perovskite quantum dot solar cells via hybrid interfacial architecture, Nat. Commun. 12 (2021) 466, https://doi.org/10.1038/s41467-020-20749-1.

[119] G. Casillas, U. Santiago, H. Barroìn, D. Alducin, A. Ponce, M. José-Yacamán, Elasticity of MoS2 sheets by mechanical deformation observed by in situ electron microscopy, J. Phys. Chem. C 119 (2015) 710–715, https://doi.org/10.1021/jp5093459.

[120] S. Wagner, S. Bauer, Materials for stretchable electronics, MRS Bull. 37 (2012) 207–213, https://doi.org/10.1557/mrs.2012.37.

[121] W. Chen, Z. Zhang, G. Liu, Retinomorphic optoelectronic devices for intelligent machine vision, iScience 25 (2022) 103729, doi:10.1016/j.isci.2021.103729.

[122] C.A. Curcio, K.A. Allen, Topography of ganglion cells in human retina, J. Comp. Neurol. 300 (1990) 5–25, https://doi.org/10.1002/cne.903000103.